

國立交通大學

電子物理研究所

博士論文

高重覆率全固態人眼安全雷射研究

Study of High-Repetition-Rate All-Solid-State

Lasers in the Eye-Safe Region

研究生： 陳思武

指導教授： 陳永富 教授

中華民國九十六年六月

高重覆率全固態人眼安全雷射研究
Study of high-repetition-rate all-solid-state lasers
in the eye-safe region

研究生：陳思武

Student : Szu-Wu Chen

指導教授：陳永富

Advisor : Yung-Fu Chen

國立交通大學
電子物理研究所
博士論文

A Thesis

Submitted to Institute and Department of Electrophysics

College of Science

National Chiao Tung University

in partial Fulfillment of the Requirements

for the Degree of

PhD

in

Institute and Department of Electrophysics

June 2007

Hsinchu, Taiwan, Republic of China

中華民國九十六年六月

高重覆率全固態人眼安全雷射研究

學生：陳思武

指導教授：陳永富

國立交通大學電子物理學系研究所博士班

摘 要

波長 $1.5\sim 1.6\ \mu\text{m}$ 的脈衝式人眼安全雷射在雷射遙測和雷射測距儀等相關應用上是不可或缺的。高重覆率($>10\text{kHz}$)高尖峰功率($>1\text{kW}$)的雷射，有助於提升應用系統的效能，而光學參數振盪器(OPO)雷射能具有這一特性。在論文裡以摻釹釷酸鈮($\text{Nd}^{3+}:\text{YVO}_4$)和鈦氧磷酸鉀(KTP)晶體為研究主體，使用 1064nm 左右的 $\text{Nd}^{3+}:\text{YVO}_4$ 雷射激發以KTP晶體為主OPO可以產生波長在 $1.57\ \mu\text{m}$ 附近的人眼安全固態雷射。分別採用聲光晶體、可飽和吸收體作為Q-開關元件(Q-switcher)，實現高轉換效率的主、被動式Q-開關脈衝型雷射系統。首先，我們完成一個採用聲光晶體Q-開關雷射二極體激發式 $\text{Nd}^{3+}:\text{YVO}_4$ /腔內OPO雷射系統，可以工作在 $10\sim 80\text{kHz}$ 高脈衝重覆率。進一步研究腔內OPO雷射輸出的最佳化，而獲得更高的功率輸出。在激發功率 15W ，脈衝重覆率 80kHz 時， 1573nm 平均功率可高於 1.5W ，尖峰功率高過 2kW 。接著，改採用 $\text{Cr}^{4+}:\text{YAG}$ 吸收晶體設計製作一套結構小巧的高功率被動式人眼安全固態雷射，再藉由考慮晶體熱透鏡效應以及調整光模與激勵光束匹配條件，從而提升在 1573nm 波長輸出功率。在輸入功率 15W 時，訊號脈衝重覆率高於 50kHz ，平均輸出功率 1.5W 以上，尖峰功率高於 5kW 。

Study of high-repetition-rate all-solid-state lasers in the eye-safe region

Student : Szu-Wu Chen

Advisors : Dr. Yung-Fu Chen

Institute and Department of Electrophysics
National Chiao Tung University

ABSTRACT

1.5–1.6 μm wavelength pulsed eye-safe lasers are indispensable for applications such as telemetry and range finders. High-peak-power ($> 1\text{ kW}$) laser with a high repetition rate ($> 10\text{ kHz}$) is beneficial to the performance of these application systems. In this thesis, we take the optical parametric oscillator (OPO) approach to accomplish a series of high-repetition-rate high-power eye-safe lasers and investigate the optimization of output power. First, we used KTP crystal to develop an intracavity OPO laser excited by a diode-pumped acousto-optically (AO) Q-switched $\text{Nd}^{3+}:\text{YVO}_4$ laser, which could be operated at high repetition rate up to 80 kHz, and higher output power was achieved by optimization of the intracavity OPO laser output coupler. With an absorbed pump power of 15W, pulse repetition rate of 80 kHz, its average output powers at 1573nm was above 1.5W and peak powers was higher than 2 kW. Second, we demonstrated a compact 2.5W-excited high-peak-power passively Q switched eye-safe solid-state laser, by using $\text{Cr}^{4+}:\text{YAG}$ saturable absorber. Furthermore, by taking the crystal thermal lensing effect into consideration and matching the optical mode and pump beam size, we scaled up the 1573 nm output power. With an incident pump power of 15 W, the compact intracavity OPO cavity produced average output power at 1573 nm up to 1.5 W and peak powers higher than 5 kW with pulse repetition rate above 50 kHz.

誌 謝

離開校園十二年以後能有緣重回到母校裡繼續研究真是人生難得的際遇，誠摯地感謝中科院長官能在人力非常窘困的情況下，敞開這扇學習之門，讓我得以努力航向嶄新的研究目標，而其中恩師 陳永富教授的指導提攜則是這段奮鬥歷程中的指引明燈。

感謝黃凱風教授、吳光雄教授、趙天生教授以及梁振民博士與林志平博士對於本篇論文深入地瞭解與探討，給予我許多的寶貴建議、提示，讓論文更為完善，也對於未來的研究之路指引出更多的觸發方向。

固態雷射實驗室是個陣容堅強的研究團隊，在老師的帶領下，成果豐碩、欣欣向榮。冠暉的實驗精神與研究成果尤其令人刮目相看，亭樺、仕璋、哲彥也已經有不錯的成績，而接棒的學弟妹們也都有孜孜不倦的好風氣，薪火相傳、蔚為優良的研究園地。

還要感謝多年來一直默默在支持著我的家人，由於有你們的鼓勵與協助，讓我能全力以赴完成課業與論文，開啟新的研究紀元。

Table of Contents

Chinese Abstract	i
English Absrtact.....	ii
Acknowledgement.....	iii
Table of Contents	iv
Figure Captions	vi
Notations	viii
Chapter 1 Introduction	1
References.....	3
Chapter 2 Q-Switched Laser and OPO Design Principles.....	6
2.1 Actively Q-Switched Laser Design Principles	6
2.2 Passively Q-Switched Laser Design Criteria.....	9
2.3 Optical Parameter Oscillator (OPO) Theorem	13
2.3.1 Oscillation Threshold Conditions	13
2.3.2 Phase Matching Condition.....	16
2.4 Thermal Effect of Laser Crystal	19
2.4.1 Thermal Fraction Limit.....	19
2.4.2 Thermal Lensing Effect	21
References.....	24
Chapter 3 Intracavity OPO Pumped by a AO Q-Switched Nd:YVO ₄ Laser....	29
3.1 Introduction.....	29
3.2 Experimental Setup.....	30

	3.3 Conclusions.....	32
	References.....	34
Chapter 4	Output Optimization of a Diode-Pumped Actively Q-Switched IOPO	39
	4.1 Introduction.....	39
	4.2 Experimental Setup.....	40
	4.3 Result and Discussion	41
	4.4 Conclusions.....	43
	References.....	44
Chapter 5	Intracavity OPO with a Passively Q-Switched Nd:YVO ₄ Laser.....	49
	5.1 Introduction.....	49
	5.2 Experimental Setup.....	50
	5.3 Result and Discussion.....	51
	5.4 Summary	52
	References.....	54
Chapter 6	Output Optimization of Diode-pumped Passively Q-Switched Nd:YVO ₄ /KTP/Cr ⁴⁺ :YAG Laser	58
	6.1 Introduction.....	58
	6.2 Experimental Setup.....	59
	6.3 Thermal Lens Effect Analysis of a Laser Crystal.....	60
	6.4 Criterion for Good Passively Q-Switching.....	62
	6.5 Experimental Results	62
	6.6 Summary	63
	References.....	65
Chapter 7	Conclusion and Future Work	71

Figure Captions

Fig.1-1 The spectral transmission characteristics of human eye and the related laser safety standards.....	4
Fig.1-2 The turning ranges for several kinds of OPO nonlinear crystal materials	5
Fig.2-1 The energy levels of a saturable absorber with the excited state absorption.....	25
Fig.2-2 Feynman diagram of three-photon optical parametric process.	25
Fig.2-3 Different cavity configurations of optical parametric oscillator (OPO).....	26
Fig.2-4 (a) Optically pumped three-level laser, and (b) three-photon optical parametric process.	27
Fig.2-5 The turning range of an OPO pumped by a 1.06 μ m Nd laser and employing a Type-II KTP crystal	28
Fig.3-1 Schematic of the intracavity OPO pumped by a cw diode-pumped AO Q-switched Nd:YVO ₄ laser	35
Fig.3-2 The average output power at 1573 nm versus the absorbed pump power for several pulse repetition rates.....	35
Fig.3-3 The peak power and pulse width at 1573 nm versus the absorbed pump power at a pulse repetition rate of 80 kHz.....	36
Fig.3-4 A typical pulse-shape at 1573 nm for a signal reflectivity of 85% on the output coupler	36
Fig.3-5 The dependence of the peak power and pulse width at 1573 nm on the pulse repetition rate at the maximum pump power of 12.6W.....	37
Fig.3-6 A typical pulse-shape at 1573 nm for signal reflectivities of a 90% and b 95% on the output coupler	38
Fig.4-1 Schematic of the actively Q-switched intracavity OPO laser.....	45
Fig.4-2 The average output power at 1573 nm as a function of the repetition for different output couplers at an absorbed pump power of 12.6W	45
Fig.4-3 Oscilloscope traces showing a train of pump and signal pulses when $R_s = 90\%$ (a), and a single pulse for pump and signal fields when $R_s = 60\%$ (b). Both results were measured at a pulse repetition rate of 80 kHz and an absorbed pump	

power of 12.6W	46
Fig.4-4 The calculated temporal profiles corresponding to the experimental results shown in Fig.3a and b, respectively.....	47
Fig.4-5 Experimental and theoretical results for the average output power versus the OPO output reflectivity at a repetition rate of 80 kHz and an absorbed pump power of 12.6W	48
Fig.4-6 Experimental and theoretical results for the output peak power versus the OPO output reflectivity at a repetition rate of 80 kHz and an absorbed pump power of 12.6W.....	48
Fig.5-1 Schematic of the intracavity OPO pumped by a diode-pumped passively Q-switched Nd : YVO ₄ /Cr ⁴⁺ : YAG laser.....	55
Fig.5-2 Dependence of the average output power and the pulse repetition rate at 1573 nm on the absorbed pump power. An oscilloscope trace of a train of the signal pulses is shown in the inset.....	55
Fig.5-3 Typical temporal shapes for the laser and signal pulses with a signal reflectivity of 80% on the output coupler.....	56
Fig.5-4 Dependence of the peak power and the pulse energy at 1573 nm on the absorbed pump power.....	56
Fig.5-5 Typical temporal shapes for the laser and signal pulses with a signal reflectivity of 90% on the output coupler.....	57
Fig.6-1 Schematic of the intracavity OPO pumped by a diodepumped passively Q-switched Nd:YVO ₄ /Cr ⁴⁺ :YAG laser.....	68
Fig.6-2 Calculation results for the dependence of the mode size ratios ω_1 / ω_p and ω_2 / ω_1 on the pump power for the present cavity configuration.	68
Fig.6-3 Dependence of the average output power at 1573 nm on the incident pump power. An oscilloscope trace of a train of the signal pulses is shown in the inset.	69
Fig.6-4 Dependence of the pulse repetition rate and the pulse energy at 1573 nm on the incident pump power. A typical temporal shape for the laser and signal pulses is shown in the inset.	69
Fig. 6-5 Typical temporal shapes for the laser and signal pulses with a signal reflectivity of 70% on the output coupler.....	70

Notations

ω	:	mode beam radius, mode size
n	:	inversion population density
c	:	speed of light
ϕ_P, ϕ_S	:	Pump and signal photon density respectively
l_{ca}	:	optical length of the laser cavity
σ	:	stimulated emission cross section
t_{rp}	:	round-trip time in the laser cavity
$\Delta\phi_P$:	spontaneous emission intensity
L	:	round-trip pump wave intensity loss in the laser cavity
R	:	global reflectivity of the laser cavity mirrors
σ_{OPO}	:	effective OPO conversion cross section
$\Delta\phi_S$:	noise signal intensity
L_S	:	round-trip signal wave intensity loss in the OPO cavity
R_S	:	output reflectivity of the OPO mirror
ω_1, ω_2	:	idler and signal frequencies, respectively
n_1, n_2, n_3	:	refractive indices at the idler, signal and pump wavelengths, respectively
d_{eff}	:	effective non-linear coefficient
ϵ_0	:	vacuum permittivity
λ	:	lwavelength
R_c	:	radius of curvature of the mirror
ξ	:	fractional thermal loading
K_c	:	thermal conductivity
P_{in}	:	incident pump power
dn/dT	:	thermal-optic coefficients of n
α_T	:	thermal expansion coefficient along the a-axis
M^2	:	beam quality factor
z_0	:	focal plane of the pump beam

ρ_1	:	radius of curvature of the mirror
T_0	:	initial transmission of the saturable absorber
A/A_s	:	ratio of the effective area in the gain medium and in the saturable absorber
σ_{gs}	:	ground-state absorption cross-section of the saturable absorber
σ_γ	:	stimulated emission cross-section of the gain medium
γ	:	inversion reduction factor with a value between 0 and 2
β	:	ratio of the excited-state absorption cross-section to that of the ground-state absorption in the saturable absorber



Chapter 1 Introduction

Nanosecond pulsed lasers emitting in the eye-safe wavelength region (1.5–1.6 μm) are indispensable for applications such as telemetry and for use in range finders [1]. High-peak-power laser sources at wavelengths greater than 1.5 μm are vital for applications involving coherent laser radar, remote sensing and active imaging [2]. In this spectral range, radiation is mostly absorbed in the ocular fluid of the eye rather than in the retina. The spectral transmission characteristics of human eye is shown in Fig.1-1. Several recommended standards are also described in the figure.[16-18] Nowadays, eye safety is an very important requirement for laser applications involving free space propagation.

The eye-safe requirement has stimulated much interest in different generation approaches. There are three methods to reach the goal : erbium (Er)-doped lasers, Raman lasers, and optical parametric oscillators (OPOs). During the past two decades, OPO has not only been proved to be a very efficient approach to manufacture an eye-safe laser, but also be a nice method to achieve an tunable laser. As depicted in Fig.1-2 ,the turning ranges for several kinds of OPO nonlinear crystal materials could cover the spectrum from visible to mid infrared region.

Even though intracavity OPOs have been proposed for over 30 years [3-5], the conventional intracavity OPOs in which flash lamps or quasi-cw diodes are used as the pump sources typically restrict operations to low repetition rates, less than 1 kHz [14-15]. Only recently OPOs merits have been noted by the availability of high-damage-threshold non-linear crystals and diode-pumped Nd-doped lasers [6-9]. Several crystals belonging to the potassium titanyl phosphate (KTP) family, when pumped by Nd-doped laser pumps around 1050–1070 nm, generate signal wavelengths around 1.55 μm [10-13]. One advantage of the KTP family is the non-critical phase-matching configuration that allows a good OPO conversion efficiency even with poor-beam-quality pump lasers. Another advantage is the large available crystal size that allows the generation of high energies. Furthermore, using a diode-pumped

Nd-doped laser to intracavity pump the OPO can offer a compact and rugged design with a low threshold and high efficiency, but at a frequency repetition rate from 1 to 20 kHz, the overall average power is less than 60mW[16].

Passively Q-switched Nd :YVO₄ and Nd : GdVO₄ lasers have been demonstrated recently[11-13], but the output pulse energy and peak power are obviously lower than those of Nd :YAG laser. Therefore, so far the pumped sources for passively Q-switched intracavity OPO's are mostly composed of Nd :YAG and Cr⁴⁺ :YAG crystals. The relatively narrow absorption band of Nd :YAG crystal, however, sets stringent requirements on the spectrum of the pump diodes.

By taking the advantage of the KTP crystal, we accomplish a series of experiments and analysis on Q-switched Nd:YVO₄ lasers. In this thesis we demonstrate a high repetition-rate intracavity OPO based on a non-critically phase-matched KTP crystal excited by a cw-diode-pumped acousto- optically (AO) Q-switched Nd:YVO₄ laser operating at 10-80 kHz. With an absorbed pump power of 12.6W, the compact intracavity OPO cavity, operating at 80 kHz, produces average powers at 1.573 μm up to 1.33W and peak powers higher than 2 kW.

A compact eye-safe optical parametric oscillator (OPO) using a noncritically phase-matched KTP crystal intracavity pumped by a passively Q-switched Nd :YVO₄ laser is also experimentally demonstrated. To enhance the performance of passive Q-switching, a Cr⁴⁺:YAG saturable absorber crystal is coated as an OPO output coupler in a nearly hemispherical cavity. With an incident pump power of 2.5W, the compact intracavity OPO cavity, operating at 62.5 kHz, produces average powers at 1573 nm up to 255 mW and peak powers higher than 1kW.

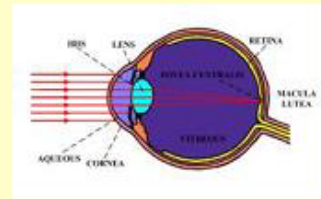
References

- [1] L.R. Marshall, A.D. Hays, J. Kasinski, R. Burnham: Proc. SPIE 1419,141 (1991)
- [2] E.O. Amman, J.M. Yarborough, M.K. Oshman, P.C.Montgomery: Appl. Phys. Lett. 16, 309 (1970)
- [3] M.K. Oshman, S.E. Harris: IEEE J. Quantum Electron. QE-4, 491(1968)
- [4] J. Falk, J.M. Yarborough, E.O. Amman: IEEE J. Quantum Electron. QE-7, 359 (1971)
- [5] R.C. Stoneman, L. Esterowitz: In: Proc. Conf. Adv. Solid State Lasers, Salt Lake City, Utah (Optical Society of America, Washington DC 1990) pp. 176–178, paper WC5-2; L.R. Marshall, A.D. Hays, J. Kasinski, R. Burnham: Proc. SPIE 1419, 141 (1991)
- [6] R. Lavi, A. Englander, R. Lallouz: Opt. Lett. 21, 800 (1996)
- [7] A.R. Geiger, H. Hemmati, W.H. Farr, N.S. Prasad: Opt. Lett. 21, 201(1996)
- [8] Y. Yashkir, H.M. van Driel: Appl. Opt. 38, 2554 (1999)
- [9] L.R. Marshall, J. Kasinski, R. Burnham: Opt. Lett. 16, 1680 (1991)
- [10] L.R. Marshall, A. Kaz: J. Opt. Soc. Am. B 10, 1730 (1993)
- [11] G. Xiao, M. Bass, M. Acharekar: IEEE J. Quantum Electron. 34, 2241(1998)
- [12] R. Dabu, C. Fenic, A. Stratan: Appl. Opt. 40, 4334 (2001)
- [13] A. Dubois, S. Victori, T. L'épine, P. Georges, A. Brun: Appl. Phys. B 67,181 (1998)
- [14] A. Agnesi, S. Dell'Acqua, G. Reali: Appl. Phys. B 70, 751 (2000)
- [15] R.S. Conroy, C.F. Rae, G.J. Friel, M.H. Dunn, B.D. Sinclair: Opt. Lett.23, 1348 (1998)
- [16] CNS 11640,Z1043 “The Safe Use of Lasers” Bureau of Standards, Metrology and Inspection (BSMI) 1999
- [17] ANSI “American National Standard for Safe Use of Lasers”, Laser Institute of America.
- [18] David H. Sliney “Guide for the Slection of Laser Eye Protection”, Laser Institute of America 1996.

Standards for safe use of Lasers

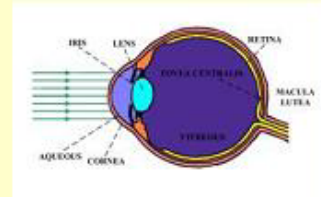
ANSI Z136.1-1993
EN 60825.1-1994
CNS 11640 Z1043

**Visible and
Near-Infrared
(400-1400 nm)**



$\lambda > 1400 \text{ nm}$

**Mid/Far-Infrared
(1400nm-1mm)
Mid-Ultraviolet
(180-315nm)**



**Near-Ultraviolet
(315-390nm)**

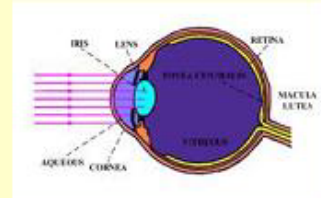


Fig.1-1 The spectral transmission characteristics of human eye and the related laser safety standards.

OPO (Optical Parametric Oscillators) Approach

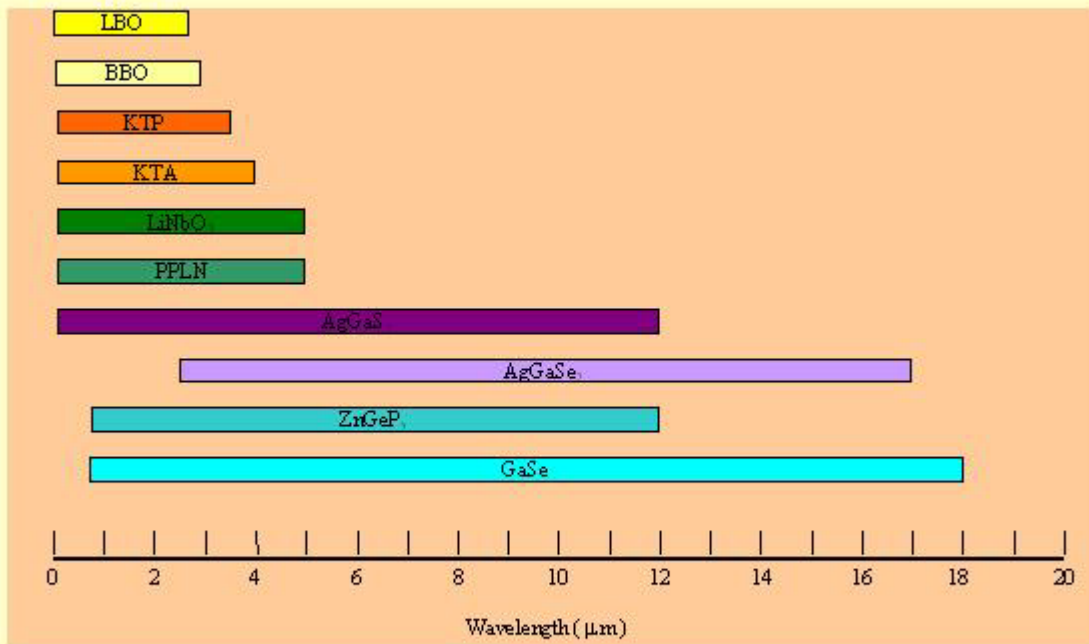


Fig.1-2 The turning ranges for several kinds of OPO nonlinear crystal materials .

Chapter 2 Q-Switched Laser and OPO Design Principles

2.1 Actively Q-Switched Laser Design Principles

The spatial variation of pumping and intracavity photon density should be taken into consideration in the rate equations for LD-pumped CW-operated or Q-switched solid-state lasers. Assume for LD-pumped CW-operated solid-state lasers, the spatial variation of pumping and intracavity photon density in the rate equations can be expressed as [1]

$$\phi(r,t) = \phi(0,t) \exp\left(-\frac{2r^2}{\omega_L^2}\right) \quad (2.1-1)$$

where $\phi(0,t)$ is the photon density along the laser axis, r is the radial coordinate, ω_L is the laser mode radius, which is determined by the geometry of the resonator.

$$\int_0^\infty \frac{d\phi(r,t)}{dt} 2\pi r dr = \int_0^\infty \frac{\phi(r,t)}{t_r} \left[2\sigma n(r,t)l - \ln\left(\frac{1}{R}\right) - L \right] 2\pi r dr \quad (2.1-2)$$

$$\frac{dn(r,t)}{dt} = -\gamma\sigma\phi(r,t)n(r,t) \quad (2.1-3)$$

where $n(r,t)$ is the population inversion density, σ and l are the stimulated emission cross section and length of the gain medium, respectively, $t_r = 2l'/c$ is the round-trip transit time of the light in the resonator of optical length l_r , c is the light speed in vacuum, R is the reflectivity of the output mirror, γ is the inversion reduction factor, which actually corresponds to the net reduction in the population inversion resulting from the stimulated emission of a single photon, and L is the remaining round-trip dissipative optical loss.

For four-level gain media like $\text{Nd}^{3+}:\text{YAG}$ and $\text{Nd}^{3+}:\text{YVO}_4$ ($1.06 \mu\text{m}$), the

pumped population is small compared to the total population, the ground state population density can be considered as constant, and assume there is no residual population inversion density from the preceding pulse is included,

$$n(r,0) = n(0,0) \exp\left(-\frac{2r^2}{\omega_p^2}\right) \quad (2.1-4)$$

where ω_p is the average radius of the pump beam in the gain medium and $n(0,0)$ is the initial population inversion density in the laser axis.

When the threshold population inversion $n_{th}(r,0)$ is small relative to the initial population inversion density $n(r,0)$, for example, $n(r,0)/n_{th}(r,0) > 2.5$, then the residual population inversion density $n(r,t_f)$ at the end of a Q-switched pulse is always small enough to be neglected.

Substituting (1) and (4) into (3) and integrating the result over time, can obtain

$$n(r,t) = n(0,0) \exp\left(-\frac{2r^2}{\omega_p^2}\right) \cdot \exp\left[-\gamma\sigma c \int_0^t \phi(0,t) dt \cdot \exp\left(-\frac{2r^2}{\omega_l^2}\right)\right] \quad (2.1-5)$$

Substituting (5) into (2) yields

$$\begin{aligned} \frac{d\phi(0,t)}{dt} = & \frac{4\sigma l}{\omega_l^2 t_r} \phi(0,t) n(0,0) \int_0^\infty \exp\left[-\alpha\sigma c \int_0^t \phi(0,t) dt \cdot \exp\left(-\frac{2r^2}{\omega_l^2}\right)\right] \\ & \cdot \exp\left[-2r^2\left(\frac{1}{\omega_p^2} + \frac{1}{\omega_l^2}\right)\right] 2r \cdot dr - \frac{\phi(0,t)}{t_r} \left[\ln\left(\frac{1}{R}\right) + L \right] \end{aligned} \quad (2.1-6)$$

The threshold of the initial population inversion density in the laser axis can derived by setting (6) equal to zero at $t = 0$.

$$n_{th}(0,0) = \frac{\ln(1/R) + L}{2\sigma l} \left(1 + \frac{\omega_l^2}{\omega_p^2}\right) \quad (2.1-7)$$

Here introduce the normalized time τ , normalized photon density $\Phi(r, \tau)$ and normalized population inversion density $N(r, \tau)$ as

$$\tau = \frac{t}{t_c} = \frac{t}{t_r} \left[\ln\left(\frac{1}{R}\right) + L \right] \quad (2.1-8)$$

$$\Phi(r, \tau) = \frac{\phi(r, \tau)}{\frac{\ln(1/R) + L}{2\gamma\sigma l'}} \quad (2.1-9)$$

$$N(r, \tau) = \frac{n(r, \tau)}{n_{th}(0,0)} \quad (2.1-10)$$

where t_c is the photon decay time, $N(0,0)$ is the ratio of the initial population inversion density in the laser axis $n(0,0)$ to the threshold $n_{th}(0,0)$.

Then, the output pulse width W , pulse peak power P_m and pulse energy E can be expressed explicitly as

$$W = (\tau_r + \tau_f) t_c = \frac{(\tau_r + \tau_f) \cdot t_r}{\ln(1/R) + L} \quad (2.1-11)$$

$$P_m = \frac{h\nu}{t_r} \ln\left(\frac{1}{R}\right) \int \phi_m dV = \frac{\pi\omega_L^2 h\nu}{4\sigma\gamma t_r} \left[\ln\left(\frac{1}{R}\right) + L \right] \cdot \ln\left(\frac{1}{R}\right) \cdot \Phi_m \quad (2.1-12)$$

$$E = \frac{h\nu}{t_r} \ln\left(\frac{1}{R}\right) \iint \phi(r, t) dV dt = \frac{\pi\omega_L^2 h\nu}{4\sigma\gamma} \ln\left(\frac{1}{R}\right) \cdot \int_0^\infty \Phi(0, \tau) d\tau \quad (2.1-13)$$

where Φ_m is the maximum value of $\Phi(0, \tau)$.

2.2 Passively Q-Switched Laser Design Criteria

Degnan has derived the key parameters of an energy-maximized passively Q-switched laser as function of two variables $\alpha = \sigma_s \gamma_s / \sigma \gamma$, and, $z = \frac{2\sigma n_i l}{L}$. Xiao and Bass, and Zhang et al. have extend the analysis to include the effect of excited state absorption (ESA) in the saturable absorber recently.

In the actively Q-switched laser the initial population density of the gain medium n_i is normally proportional to the pump rate. So it is suitable in practice to optimize the output pulse energy with the variable z . However, for the passively Q-switched laser, it is not in the same case, n_i is determined by the initial transmission of the saturable absorber (T_0) and the reflectivity of the out put mirror (R).

The coupled rate equations for three or four level gain media are given by [2]

$$\frac{d\phi}{dt} = \frac{\phi}{t_r} [2\sigma n l - 2\sigma_{gs} n_{gs} l_s - 2\sigma_{es} n_{es} l_s - (\ln(\frac{1}{R}) + L)] \quad (2.2-1)$$

$$\frac{dn}{dt} = -\gamma c \sigma \phi n \quad (2.2-2)$$

$$\frac{dn_{gs}}{dt} = -\frac{A}{A_s} c \sigma_{gs} \phi n_{gs} \quad (2.2-3)$$

$$n_{so} = n_{gs} + n_{es} \quad (2.2-4)$$

where

ϕ is the intracavity photon density with respect to the effective cross-sectional area of the laser beam in the gain medium;

n is the population density of the gain medium;

l is the length of the gain medium;

σ is the stimulated emission cross sections of the gain medium;

l_s is the length of the saturable absorber;

A/A_s is the ratio of the effective area in the gain medium and in the saturable absorber;

n_{gs} , n_{es} are the population density of absorber ground state and excited state, respectively;

n_{so} is the total population density of absorber;

σ_{gs} , σ_{es} are the GSA and ESA cross sections in the saturable absorber, respectively;

R is the reflectivity of the output mirror;

γ is the inversion reduction factor and equal to 1,2 for four-level and three-level systems, respectively;

L is the nonsaturable intracavity round-trip dissipative optical loss;

t_r is the round-trip transit time of light in the cavity, equal to $2l'/c$, where l' is the cavity optical length, c is the speed of light.

In the equations (3)-(4), the saturable absorber is considered as a four level system, including the excited state, as illustrated in the Fig. 2-1.

It is interesting to solve these above equations to get the conclusion about the influence of excited-state absorption. And the intracavity focusing effect on the threshold condition and output characteristics.

Dividing (2) by (3) and integrating gives

$$n_{gs} = n_{so} \left(\frac{n}{n_i} \right)^\alpha \quad (2.2-5)$$

where

$$\alpha = \frac{1}{\gamma} \frac{\sigma_{gs}}{\sigma} \frac{A}{A_s} \quad (2.2-6)$$

n_i is the initial population inversion density in the gain medium and n_i can be calculated from equation (1), by setting the round-trip net gain equal to zero just before the Q-switch opens.

$$2\sigma n_i l - 2\sigma_{gs} n_{so} l_s - \left(\ln\left(\frac{1}{R}\right) + L\right) = 0 \quad (2.2-7)$$

To point out the correspondence with the previous analysis, we can use the following expression:

$$T_o = \exp(-\sigma_{gs} n_{so} l_s) \quad (2.2-8)$$

Where T_o is the initial transmission of the saturable absorber. Then

$$n_i = \frac{\ln\left(\frac{1}{T_o^2}\right) + \ln\left(\frac{1}{R}\right) + L}{2\sigma l} \quad (2.2-9)$$

Dividing (1) by (2) and substituting (5) into the result gives

$$\frac{d\phi}{dn} = -\frac{l}{\gamma l'} \left[1 - \frac{1-\beta}{2\sigma n_i l} \ln\left(\frac{1}{T_o^2}\right) \left(\frac{n}{n_i}\right)^{\alpha-1} - \frac{\beta \ln\left(\frac{1}{T_o^2}\right) + \ln\left(\frac{1}{R}\right) + L}{2\sigma l n} \right] \quad (2.2-10)$$

where

$$\beta = \frac{\sigma_{es}}{\sigma_{gs}} \quad (2.2-11)$$

Since the first derivative of ϕ with respect to n at $n = n_i$ is equal to zero, the criterion for Q-switching behavior is whether the second derivative has a positive or a negative sign. If positive, the growth curve for the photon intensity will turn increasingly upward.

$$\frac{d^2\phi}{dn^2} = -\frac{l}{\gamma l'} \left[-\frac{(1-\beta)(\alpha-1)}{2\sigma l n_i^2} \ln\left(\frac{1}{T_o^2}\right) \left(\frac{n}{n_i}\right)^{\alpha-2} + \frac{\beta \ln\left(\frac{1}{T_o^2}\right) + \ln\left(\frac{1}{R}\right) + L}{2\sigma l n^2} \right] \quad (2.2-12)$$

Substituting n and n_i into (12), the criterion for a giant pulse to occur is then given

by

$$[\alpha(1-\beta)-1]\ln\left(\frac{1}{T_0^2}\right)-\ln\left(\frac{1}{R}\right)-L > 0 \quad (2.2-13)$$

Substituting (6) into (13), the criterion for the second threshold becomes

$$\frac{\ln\left(\frac{1}{T_0^2}\right)}{\ln\left(\frac{1}{T_0^2}\right)+\ln\left(\frac{1}{R}\right)+L} \frac{\sigma_{gs}}{\sigma} \frac{A}{A_s} > \frac{\gamma}{1-\beta} \quad (2.2-14)$$

Note that the parameters α and β are determined from the cavity configuration and the physical properties of the gain medium and the saturable absorber. It becomes very straightforward that the more the α value greater than 1, or the closer the β value to 0, the easier the equation (14) to keep true. From this equation, we can derive the permissible max. T_0 value or min. R value to satisfy the criterion.



2.3 Optical Parameter Oscillator (OPO) Theorem

Optical parameter process is one of the fundamental nonlinear optical processes. It involves three photons in the process, and can be depicted schematically by a Feynman diagram, as shown in Fig.2-2. In the process, one high-frequency photon is annihilated and two lower-frequency photons are created. In other words, the optical parametric process can be put in a resonant cavity to form an optical parameter oscillator (OPO) to generate two different waves, called signal and idler wave, by one wave, called pump wave. Fig.2-3 illustrates different cavity configurations of OPO. In some way, the characteristics of OPO's are very similar to the optically-pumped 3-level laser as shown in Fig.2-4. However there are a number of differences. For the OPO's, the middle energy level can be tuned through the phase-matching condition, and the top energy level can be tuned by changing the pump frequency. Since the laser involves three single-step resonant transitions while the parametric process involves a three-photon transition, the threshold for oscillation is generally much higher for OPO's than that for the lasers.

2.3.1 Oscillation Threshold Conditions

To derive the OPO oscillation threshold conditions, we consider the most general case of singly-resonant oscillator. The basic oscillator configuration is consist of a plane-plane (Fabry-Perot)cavity with a nonlinear crystal put inside. Then the Oscillation threshold conditions can be derived from solving the signal and idler's coupled-wave equations and coupled-amplitude equations by substituting the suitable boundary conditions. [3, 4]

The wave equation for E-field in the nonlinear optical medium is described by

$$\nabla^2 E(r,t) - \mu_0 \varepsilon_0 \frac{\partial^2}{\partial t^2} E(r,t) = \frac{4\pi}{c^2} \frac{\partial^2}{\partial t^2} P(r,t) \quad (2.3-1)$$

In the case of basic three-photon parametric process,

$$E(r,t) = \frac{1}{2} \left\{ E_1(r) e^{i(k_1 \cdot r - \omega_1 t)} + E_2(r) e^{i(k_2 \cdot r - \omega_2 t)} + E_3(r) e^{i(k_3 \cdot r - \omega_3 t)} \right. \\ \left. + \text{complex conjugates} \right\} \quad (2.3-2)$$

$$P(r,t) = \frac{1}{2} \left\{ P^L(r,t) + P^{NL}(r,t) + \text{complex conjugates} \right\} \quad (2.3-3)$$

where

$$P^L(r,t) = \chi^{(1)}(\omega_1) E_1(r) e^{i(k_1 \cdot r - \omega_1 t)} + \chi^{(1)}(\omega_2) E_2(r) e^{i(k_2 \cdot r - \omega_2 t)} + \chi^{(1)}(\omega_3) E_3(r) e^{i(k_3 \cdot r - \omega_3 t)} \quad (2.3-4)$$

$$P^{NL}(r,t) = \chi^{(2)}(\omega_3) : E_1 E_2^* e^{i((k_1 - k_2) \cdot r - \omega_3 t)} + \chi^{(2)}(\omega_2) : E_1 E_3^* e^{i((k_1 - k_3) \cdot r - \omega_2 t)} \\ + \chi^{(2)}(\omega_1) : E_2 E_3 e^{i((k_2 + k_3) \cdot r - \omega_1 t)} \quad (2.3-5)$$

For the linear amplification regime, the depletion of the pump wave can be neglected. We can obtain from the above equations the coupled-wave equations for the signal and idler waves

$$\left[\frac{\partial^2}{\partial z^2} + \frac{(n_2 \omega_2)^2}{c^2} \right] E_2(z) e^{ik_2 z} = -\frac{4\pi \omega_2^2}{c^2} d_{eff} E_p E_3^* e^{ik_2 z} \\ \left[\frac{\partial^2}{\partial z^2} + \frac{(n_3 \omega_3)^2}{c^2} \right] E_3(z) e^{ik_3 z} = -\frac{4\pi \omega_3^2}{c^2} d_{eff} E_p E_2^* e^{ik_3 z} \quad (2.3-6)$$

where d_{eff} is the effective Kleinman d-coefficient

$$d_{eff} = \sum_{i,j,k=1}^3 \chi_{ijk}^{(2)} \varepsilon_{2i} \varepsilon_{pj} \varepsilon_{3k} \quad (2.3-7)$$

ε_{pj} is the direction cosine of the \hat{E}_i with respect to \hat{j} -axis

$\chi_{ijk}^{(2)}$ refers to frequency-mixing process

In the slowly-varying amplitude condition, the coupled second-order differential equations can be solved more easily. Then

$$\begin{aligned}\frac{\partial}{\partial z} E_2(z) &= i \left(\frac{2\pi k_2}{n_2^2} \right) d_{eff} E_p E_3^*(z) \\ \frac{\partial}{\partial z} E_3(z) &= i \left(\frac{2\pi k_3}{n_3^2} \right) d_{eff} E_p E_2^*(z)\end{aligned}\tag{2.3-8}$$

Combing the above two equations

$$\begin{aligned}\frac{\partial^2}{\partial z^2} E_2(z) &= \frac{(2\pi)^2 k_2 k_3 |d_{eff}|^2 |E_p|^2}{n_2^2 n_3^2} E_2(z) \\ &= g^2 E_2(z)\end{aligned}\tag{2.3-9}$$

where g is defined as the spatial gain coefficient.

This equation could be solved under the boundary conditions $E_i(0)$ and $E_s(0)$.

Lead to

$$\begin{aligned}E_s(z) &= E_s(0) \cosh gz + i \frac{n_i}{n_s} \sqrt{\frac{k_s}{k_i}} E_i^*(0) \sinh gz \\ E_i(z) &= E_i(0) \cosh gz + i \frac{n_s}{n_i} \sqrt{\frac{k_i}{k_s}} E_s^*(0) \sinh gz\end{aligned}\tag{2.3-10}$$

Assume the crystal length is L , and the reflectivity of the OPO cavity mirrors are r_1 and r_2 , respectively, so the boundary conditions are $E_i(0) = 0$ and $E_s(0) = r_1 r_2 E_s(L)$.

Then, the oscillation condition is

$$E_s(L) = E_s(0) \cosh gL = r_1 r_2 E_s(L) \cosh gL\tag{2.3-11}$$

It can be rewrote as

$$1 = r_1 r_2 \cosh gL\tag{2.3-12}$$

2.3.2 Phase Matching Condition

The efficiency of generation of idler or signal waves from the nonlinear polarization in matter is dependent on the overlap situation. When the incident pumping light is oriented with respect to the crystal in a suitable condition such that the wave and the newly generated waves are in suitable phase over the interaction length, it is called phase matching. It can be achieved in the anisotropic materials, like crystals, basing on the birefringence property.

OPO is a three-photon parametric process as depicted before. Although it is a nonlinear optical process, it is still based on the energy and momentum conservation theorem[5]. From the energy conservation theorem

$$h\nu_p = h\nu_s + h\nu_i \quad (2.3-13)$$

it implies

$$\frac{1}{\lambda_p} = \frac{1}{\lambda_s} + \frac{1}{\lambda_i} \quad (2.3-14)$$



For significant parametric amplification, the generated polarization waves should be travel at the same velocity, which implies the k vectors or refractive indices for the waves in the material need to satisfy the momentum-matching condition, i.e.

$$k_p = k_s + k_i \quad (2.3-15)$$

and for collinearly condition, it implies

$$\frac{n_p}{\lambda_p} = \frac{n_s}{\lambda_s} + \frac{n_i}{\lambda_i} \quad (2.3-16)$$

where n_p, n_s and n_i are the refractive indices at pump, signal and idler frequency, respectively.

Since the refractive indices are function of the direction, wavelength and polarization, phase matching condition can be achieved by using birefringence and dispersion method. In generally, it can be reached by angle or temperature turning of the crystal. In high power applications, the second method is more difficult to be achieved, because of residual absorption in the crystal.

There are two type of phase matching. In the case of the signal and idler are ordinary rays, it is called type I phase matching. In other case, if either one is an extraordinary ray, it is referred to as type II phase matching.

The turning curves for parametric oscillators can be analyzed and figured out by solving the phase matching equations. Nevertheless, the indices of refraction should be known over the whole turning range in advance. Now take the KTP crystal as an example. The principle axes of the index ellipsoid are used to defined such that $n_x < n_y < n_z$, the indices of reflection for the ray propagation in the direction of $k, (\theta, \phi)$ can be calculated by

$$\frac{k_x^2}{(n_{\omega_j}^{-2} - n_{x,\omega_j}^{-2})} + \frac{k_y^2}{(n_{\omega_j}^{-2} - n_{y,\omega_j}^{-2})} + \frac{k_z^2}{(n_{\omega_j}^{-2} - n_{z,\omega_j}^{-2})} = 0, \quad j = p, s, i \quad (2.3-17)$$

where $k_x = \sin \theta \cos \phi, k_y = \sin \theta \sin \phi, k_z = \cos \theta$

and the n_x, n_y, n_z at ω_j frequency can be pre-calculated from the appropriate Sellmeier equation.

$$\begin{aligned} n_x^2 &= 3.0065 + \frac{0.03901}{\lambda^2 - 0.04251} - 0.01327\lambda^2 \\ n_y^2 &= 3.0333 + \frac{0.04154}{\lambda^2 - 0.04547} - 0.01408\lambda^2 \\ n_z^2 &= 3.3134 + \frac{0.05694}{\lambda^2 - 0.05658} - 0.01682\lambda^2 \end{aligned} \quad (2.3-18)$$

For type-I interaction, phase matching condition is achieved by

$$\omega_p n_{op1} = \omega_s n_{os2} + \omega_i n_{oi2} \quad (2.3-19)$$

For type-II interaction,

$$\omega_p n_{op1} = \omega_s n_{os1} + \omega_i n_{oi2} \quad (2.3-20)$$

or

$$\omega_p n_{op1} = \omega_s n_{os2} + \omega_i n_{oi1} \quad (2.3-21)$$

The turning range of an OPO pumped by a 1.06 μ m Nd laser and employing a Type-II KTP crystal ($\phi=0^\circ$) is shown in Fig.2-5.



2.4 Thermal Effect of Laser Crystal

2.4.1 Thermal Fraction Limit

In the past one decade, some of neodymium-doped vanadium-based crystals have been proved to be promising candidate for diode-pumped solid state laser gain medium. These crystals include yttrium orthovanadate (YVO₄), gadolinium orthovanadate (GdVO₄), etc.. In comparison to the Nd:YAG crystals, these crystals have several advantages, for example, a bigger gain cross section, a wider absorption bandwidth, lower threshold, and polarized output.

On the other hand, from the maximum output power point of view, vanadate laser host materials have some shortages. First, their thermal conductivity is lower than that of Nd:YAG crystals, There are a lot absorbed pump power, were accumulated around the pumping region, consequently the maximum laser output power for end-pumped solid-state laser is limited by thermal fracture of laser crystals. For a conventional 1.1 at.%Nd:YVO₄ crystal the maximum permissible pumping power is limited to approximately 13.5W, in the contrast, Nd:YAG is 50-70W. Second, the absorption coefficient of is about five times that of a Nd:YAG crystal at a pump wavelength of a 1.0 at.% Nd:YVO₄ crystal it leads to a high slope coefficient, but results in a larger temperature gradient and thermal stress at the pump end. Consequently, the thermal fracture limit is lower.

However these constraints can be relieved by decreasing the dopant concentration to extend the fracture-limited pump power, at the same time, still keeping have pump absorption coefficients. By making trade-off between the fracture-limited pump power and the maximum output slope efficiency.

For fiber-coupled pump beam, $r_p(x, y, z)$ can be approximately describer as a top-hat distribution. [5,6,8]

$$r_p(x, y, z) = \frac{\alpha e^{-\alpha z}}{\pi \omega_p^2(z) [1 - e^{-\alpha l}]} \Theta(\omega_p^2(z) - x^2 - y^2) \quad (2.4-1)$$

where $\omega_p(z)$ is the pump beam waist in the gain medium,

is the absorption coefficient at the pump wavelength,

Θ is the Heaviside step function.

In the conventional edge cooling conditions, this type of pump profile leads to a steady-state temperature distribution with a parabolic and logarithmic profile inside and outside the pumped region respectively, i.e.

$$\begin{aligned}\Delta T(r, z) &= T(r_b, z) \\ &= \frac{\xi P_{abs}}{4\pi K_c} \cdot \frac{\alpha e^{-\alpha z}}{1 - e^{-\alpha l}} \left\{ \left[\left(1 - \frac{r^2}{\omega_p^2(z)} \right) + \ln \left(\frac{r_b^2}{\omega_p^2(z)} \right) \right] \cdot \Theta(\omega_p^2(z) - r^2) \right. \\ &\quad \left. + \ln \left(\frac{r_b^2}{r^2} \right) \cdot \Theta(r^2 - \omega_p^2(z)) \right\}\end{aligned}\quad (2.4-2)$$

where P_{abs} is the absorber pump power, is the fractional thermal loading the laser crystal, and l is the crystal length.

Based on the plan stress approximation, the plane stress solutions in the laser crystal can be solved analytically. Then, in the general case, $\alpha l \gg 1$ and $\omega_p/r_b \leq 1/2$, the maximum tensile stress σ_{max} is given by

$$\begin{aligned}\sigma_{max} &= \alpha_r E \frac{\xi P_{abs}}{4\pi K_c} \cdot \frac{\alpha}{1 - e^{-\alpha l}} \left[1 - \frac{1}{2} \left(\frac{\omega_p(z)}{r_b} \right)^2 \right] \\ &\approx \frac{\alpha_r E \xi P_{abs} \alpha}{4\pi K_c}\end{aligned}\quad (2.4-3)$$

where E is Young's modulus and α_r is the coefficient of thermal expansion.

Hence, the thermal fracture limited absorbed pump power is given by

$$P_{abs,limit} = \frac{1}{\alpha} \cdot \frac{4\pi R_T}{\xi}\quad (2.4-4)$$

Where $R_T = \frac{K_c \sigma_{max}}{\alpha_T E}$ is the thermal shock parameter of laser crystal.

2.4.2 Thermal Lensing Effect

For a pumped laser rod, the refractive power is grown from the central heating effect and edge cooling induced temperature distribution. The radial dependence of the index of refraction can be described as [5,9]

$$n(r) = n_0(1 - \gamma r^2) \quad (2.4-5)$$

Where n_0 is the index of refraction at the center, r is the radial position, γ is a positive parameter.

To a first approximation, the refraction power D of a rod of length l is given by

$$D = 2\gamma n_0 l \quad (2.4-6)$$

The refraction power is related to the dissipated heat P_H by

$$D = \frac{1}{k2\pi b^2} \left[\frac{dn}{dT} + \varepsilon \right] \cdot P_H \quad (2.4-7)$$

$$P_H = \chi \eta_{exc} P_{ele} \quad (2.4-8)$$

Where K is the thermal conductivity

dn/dT is the temperature derivative of the index of refraction

ε is the stress dependent variation of the index of refraction

χ is the thermal load

η_{exc} is the excitation efficiency

b is the radius

For a thermal lens with the index refraction given by (2.4-5), the ray transfer matrix is

$$M_{TL} = \begin{bmatrix} 1 - Dh & l/n_0 \\ -D & 1 - Dh \end{bmatrix} \quad (2.4-9)$$

where

$$D = 2\gamma n_0 l \quad (2.4-10)$$

$$h = l/(2n_0) \quad (2.4-11)$$

The ray transfer matrix for a resonator with a thick lens is given by

$$M_D = \begin{bmatrix} g_1^* & L^* \\ \frac{g_1^* g_2^* - 1}{L^*} & g_2^* \end{bmatrix} \quad (2.4-12)$$



Where

$$g_i^* = g_i - D \cdot d_j (1 - d_i / R_i) \quad i, j = 1, 2; i \neq j \quad (2.4-12a)$$

$$g_i = 1 - (d_1 + d_2) / R_i \quad (2.4-12b)$$

$$L^* = d_1 + d_2 - D d_1 d_2 \quad (2.4-12c)$$

$$D = \frac{1}{f} : \text{refractive power} \quad (2.4-12d)$$

Beam radius at mirrors:

$$\omega_i^2 = \frac{\lambda L^*}{\pi} \sqrt{\frac{g_j^*}{g_i^*(1-g_1^*g_2^*)}} \quad (2.4-13)$$

Waist radii:

$$\omega_{oi}^2 = \frac{\lambda L^*}{\pi} \frac{\sqrt{g_1^*g_2^*(1-g_1^*g_2^*)}}{g_j^*(L^*/\rho_i)^2 + g_i^*(1-g_1^*g_2^*)} \quad (2.4-14)$$

Beam radius at the principal planes:

$$\omega_L^2 = \left[\left(1 - \frac{d_1}{\rho_1}\right)^2 + \left(\frac{d_1}{L^*}\right)^2 \frac{g_1^*(1-g_1^*g_2^*)}{g_2^*} \right] \quad (2.4-15)$$

For a fiber-coupled laser diode, the thermal lens power can be derived by [7]

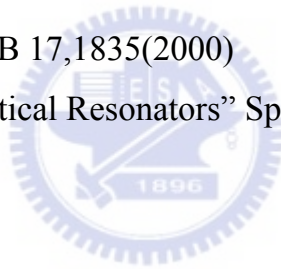
$$D = \frac{\xi P_{abs}}{2\pi K_C} \frac{[dn/dT + (n-1)\alpha_T]}{\omega_{pa}^2} \quad (2.4-16)$$

where ω_{pa} is the average pump size in the active medium, it can be expressed by

$$\begin{aligned} \omega_{pa}^2 &= \int_0^l \frac{\alpha e^{-\alpha z}}{1 - e^{-\alpha l}} \cdot \frac{1}{\omega_p^2(z)} dz \\ &= \int_0^l \frac{\alpha e^{-\alpha z}}{1 - e^{-\alpha l}} \cdot \frac{1}{\omega_{p0}^2 \left\{ 1 + \left[\frac{\lambda_p M_p^2}{n\pi\omega_{p0}^2} (z - z_0) \right]^2 \right\}} dz \end{aligned} \quad (2.4-17)$$

References

- [1] X. Zhang, S. Zhao .Q. Wang,B. Ozygus, H. Weber: IEEE Quantum Electron. QE-35,1912 (1999)
- [2] Y.F. Chen, Y.P. Lan, H.L. Chang : IEEE Quantum Electron. QE-37,462 (2001)
- [3] Ralf Menzel “Photnics :Linear and Nonlinear Interactions of Light and Matter” , Springer-Verlag 2001
- [4] C.L.Tan and L.K.Chen “Fundamentals of Optical Parametric Processes and Oscillators”
- [5] Walter Koechner “Solid-State Laser Engineering”, 5th edition ,Springer-Verlag
- [6] Y.F. Chen: IEEE Quantum Electron. QE-35,234 (1999)
- [7] Y.F. Chen, T.M. Hung, C.C. Liao, Y.P.Lan, S.C. Wang:IEEE Photon. Tech. Lett. 11,1241(1999)
- [8] Y.F. Chen:J. Opt. Soc. Am. B 17,1835(2000)
- [9] N. Hodgson ,H. Weber “Optical Resonators” Springer-Verlag 1997



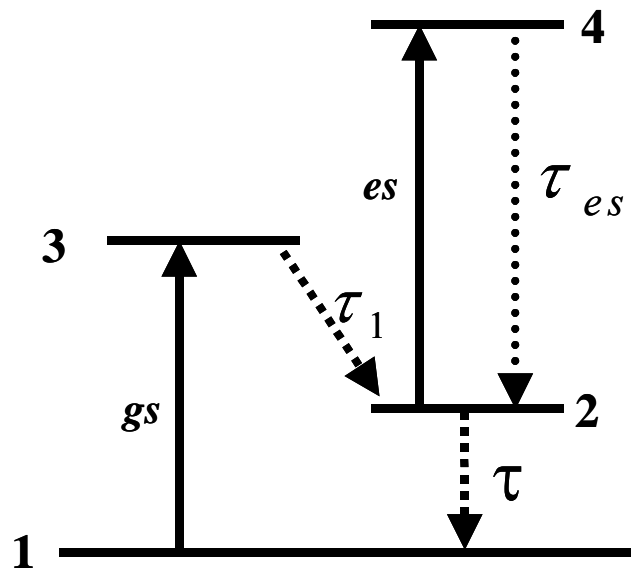


Fig.2-1 The energy levels of a saturable absorber with the excited state absorption.

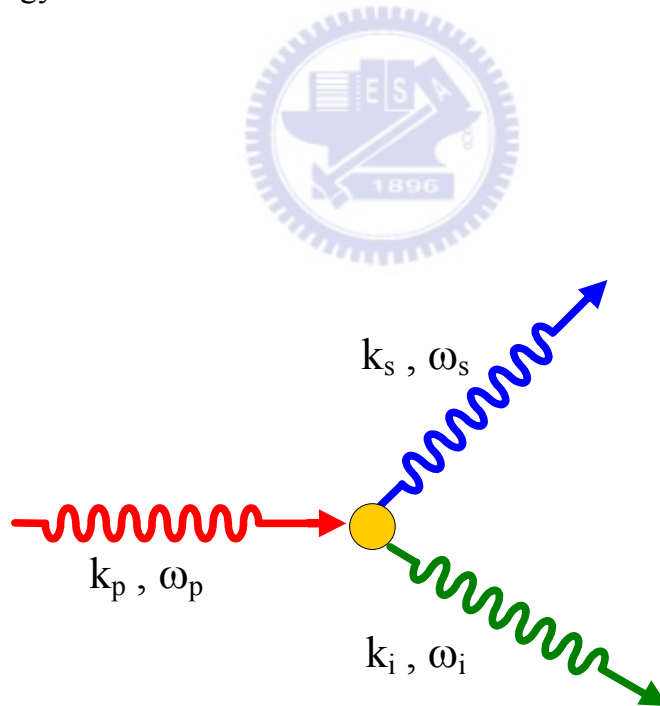
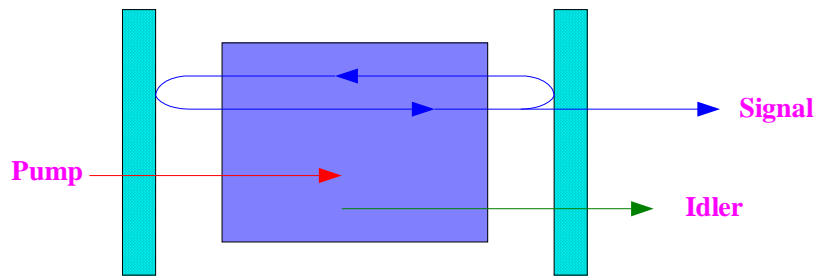
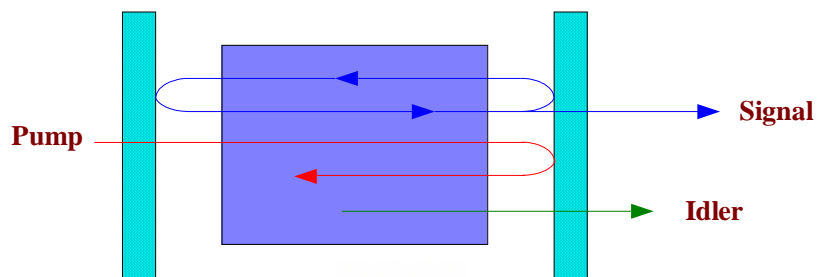


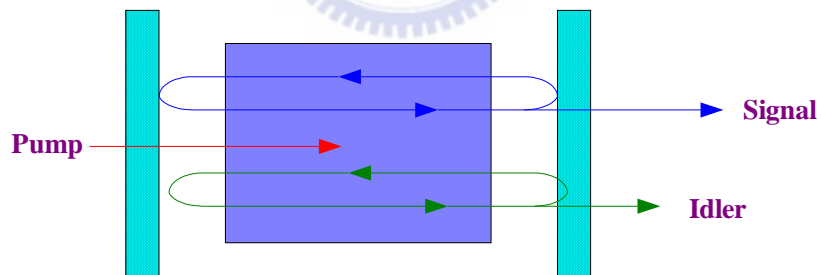
Fig.2-2 Feynman diagram of three-photon optical parametric process.



Singly Resonant OPO (SRO)



Singly Resonant Oscillator with
Pump Beam Reflected



Doubly Resonant OPO (DRO)

Fig.2-3 Different cavity configurations of optical parametric oscillator (OPO).

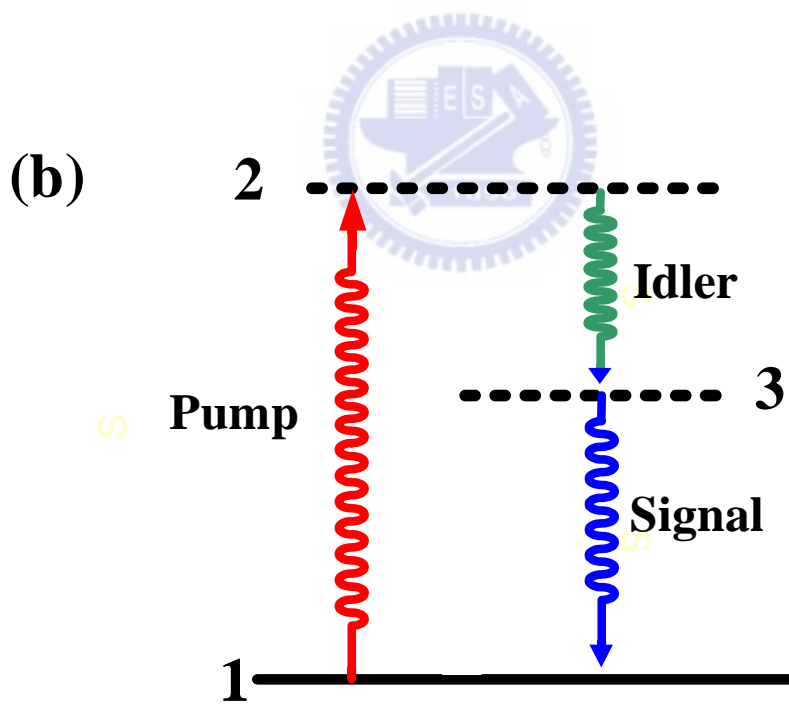
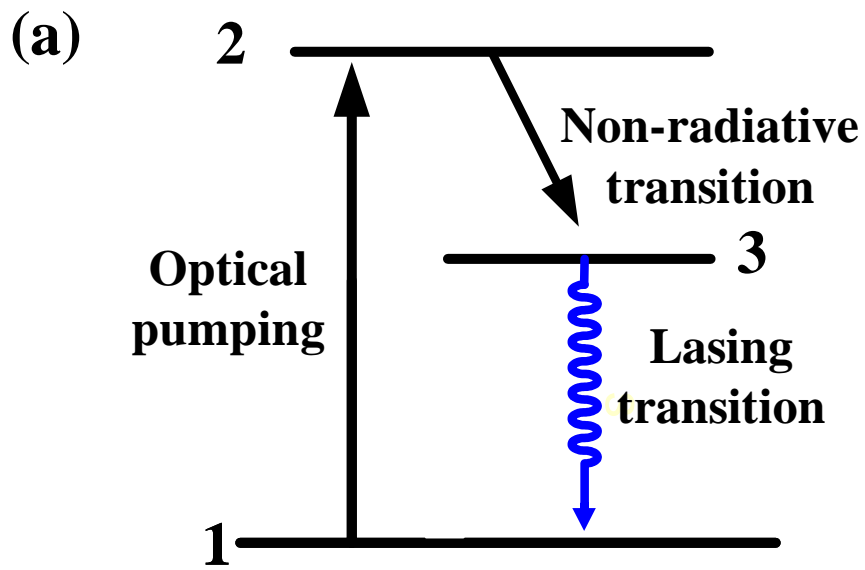


Fig.2-4 (a) Optically pumped three-level laser, and (b) three-photon optical parametric process.

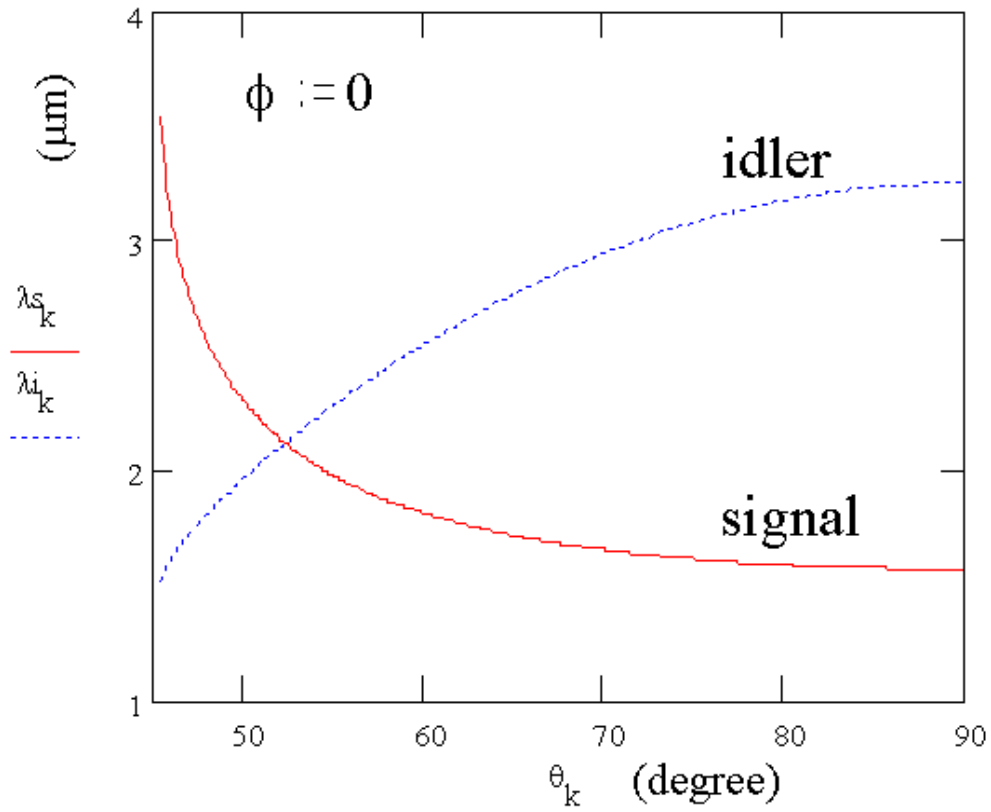


Fig.2-5 The turning range of an OPO pumped by a $1.06 \mu\text{m}$ Nd laser and employing a Type-II KTP crystal .

Chapter 3 Intracavity OPO Pumped by a AO Q-Switched Nd:YVO₄ Laser

3.1 Introduction

Nanosecond pulsed lasers emitting in the eye-safe wavelength region (1.5–1.6 μm) are indispensable for applications such as telemetry and for use in range finders [1]. The need for high-peak-power eye-safe laser sources has stimulated much interest in intracavity optical parametric oscillators (OPO's). Intracavity OPO's take advantage of a high power level within the oscillator to allow a low threshold and high efficiency compared to extracavity OPO's. Although intracavity OPO's have been proposed for over 30 years [2–4], only recently have their merits been appreciated, with the advent of high-damage-threshold nonlinear crystals and diode pumped Nd-doped lasers [1, 5–7]. Several crystals belonging to the potassium titanyl phosphate (KTP) family, when pumped by Nd-doped laser pumps around 1050–1070 nm, generate signal wavelengths around 1.55 μm [8–11]. One advantage of the KTP family is the non-critical phase-matching configuration that allows a good OPO conversion efficiency even with poor-beam-quality pump lasers. Another advantage is the large available crystal size that allows the generation of high energies. Furthermore, using a diode-pumped Nd-doped laser to intracavity pump the OPO can offer a compact and rugged design with a low threshold and high efficiency. The conventional intracavity OPO's, in which flash lamps or quasi-cw diodes are used as the pump sources, typically restrict operations to low repetition rates less than 1 kHz [12, 13]. Even though a compact diode-pumped Q-switched intracavity OPO has been demonstrated at frequency repetition rates from 1 to 20 kHz, the overall output peak power was less than 70W[14]. A recent study has shown that a high-peak-power (> 1 kW) laser with a high repetition rate (>10 kHz) is beneficial to the performance of a scanning, photon-counting laser altimeter [15]. In this work, we report the demonstration of a high repetition-rate intracavity OPO based on a non-critically phase-matched KTP crystal excited by a cw-diode-pumped acousto-optically (AO) Q-switched Nd:YVO₄

laser operating at 10 ~ 80 kHz. With an absorbed pump power of 12.6W, the compact intracavity OPO cavity, operating at 80 kHz, produces average powers at 1.573 μm up to 1.33W and peak powers higher than 2 kW.

3.2 Experimental Setup

A schematic of the basic laser setup is shown in Fig. 3-1. The experimental setup makes use of a 0.8mm core fiber with a numerical aperture of 0.16 and a maximum output power of 15W. A focusing lens with a 12.5mm focal length and 85% coupling efficiency was used to re-image the pump beam into the laser crystal. The waist diameter of the pump beam was around 300 μm . The fundamental cavity was formed by a coated Nd:YVO₄ crystal and an output coupler. The a-cut 0.3 at.% Nd³⁺, 7-mm-long Nd:YVO₄ crystal was coated for high reflectivity at 1064 nm ($R > 99.9\%$) and high transmission at 808 nm ($T > 95\%$) on one side. The other side was anti-reflection coated at 1064 nm. A Nd:YVO₄ crystal with only a low doping concentration was used to avoid the thermally induced fracture [16]. The output coupler had a dichroic coating that was highly reflective at 1064 nm ($R > 99.8\%$) and 85% partially reflective at 1573 nm. The 20-mm-long AO Q-switcher (Gooch and Housego) had antireflectance coatings at 1064 nm on both faces and was driven at a 40.68MHz center frequency with 3.0W of rf power. The OPO cavity was formed by a coated KTP crystal and an output coupler. The 20-mm-long KTP crystal was used in a type II non-critical phase-matching configuration along the x-axis ($\theta = 90^\circ$ and $\phi = 0^\circ$), to have both a maximum effective nonlinear coefficient and no walk-off between the pump, signal, and idler beams. The KTP crystal was coated to have high reflectivity at the signal wavelength of 1573 nm ($R > 99.8\%$) and high transmission at the pump wavelength of 1064 nm ($T > 95\%$). The other face of the KTP crystal was antireflection coated at 1573 nm and 1064 nm. Both the Nd:YVO₄ and KTP crystals were wrapped with indium foil and mounted in a water-cooled copper block. The water temperature was maintained at 25°C. The overall Nd:YVO₄ laser cavity length was 65mm and the OPO cavity length was 25mm.

The present flat-flat cavity was stabilized by the thermally induced lens in the laser crystal. This concept was found at nearly the same time by Zayhowski [17] and by Dixon et al. [18]. However, an end-pump-induced thermal lens is not a perfect lens, but is rather an aberrated lens. The thermally induced diffraction losses have been found to rapidly increase with the increase of the mode-to-pump size ratio at a given pump power [19]. In practice, the optimum mode-to-pump ratio is in the range of approximately 0.8–1.0 when the incident pump power is greater than 5W. In fact, the present cavity configuration has been applied to a diode-pumped Q-switched intracavity frequency-doubled Nd:YVO₄/KTP green laser [16]. It has been experimentally and theoretically shown that an excellent mode matching can be obtained for pump powers in the range 5-20W at a cavity length of approximately 60-70 mm.

To avoid damage to the intracavity optical components, the Q switcher was operated above 10 kHz. Fig.3-2 shows the operation of the intracavity OPO for several pulse repetition rates. Over this entire frequency range and for all pump powers the beam quality M^2 factor was found to be less than 1.3. The threshold for signal parametric oscillation was approximately 3-4W and its dependence on different pulse repetition rates was not significant. At a repetition rate of 10 kHz, the average output power at 1573 nm was almost saturated to 0.26W beyond 2.5 times the OPO threshold. In other words, the signal pulse energy was nearly saturated to 26 μ J beyond 2.5 times the OPO threshold. Although the maximum signal pulse energy is limited for the present cavity, increasing the pulse repetition rate can efficiently increase the average signal output power, as shown in Fig.3-2. At a pulse repetition rate of 80 kHz, the average signal power was up to 1.33W with an absorbed pump power of 12.6W. The conversion efficiency from diode laser input power to OPO signal output power was 10.6% and the corresponding slope efficiency reached 15.5%. To the best of our knowledge, this is the highest efficiency for average power conversion reported to date.

The pulse temporal behavior at 1573 nm was recorded by a LeCroy 9362 digital oscilloscope (500MHz bandwidth) with a fast germanium photodiode. Fig.3-3 depicts the peak power and pulse width versus the absorbed pump power at a pulse repetition rate of 80 kHz. A typical 1573 nm pulse is shown in Fig.3-4. It can be seen that the overall pulse width was shorter than 10 ns at a pulse repetition rate of 80 kHz. The

relatively short signal pulse indicates that the OPO effectively cavity dumps the laser energy. The striking feature is that with a 12.6W absorbed pump power, the signal peak power can be higher than 2 kW at a pulse repetition rate of 80 kHz. Fig.3-5 shows the dependence of the peak power and pulse width at 1573 nm on the repetition rate at a pump power of 12.6W. Once again, the increase in the pulse width with increasing pulse repetition rate was not significant because of the effective cavity dump of the intracavity OPO. It can be seen that the pulse width slightly increased from 5 to 8 ns as the repetition rate varied from 10 to 80 kHz. As a result of the relatively short pulse, the peak power was generally on the order of several kilowatts at pulse repetition rates from 10 to 80 kHz. Finally, experimental results reveal that the maximum signal pulse energy mainly depends on the signal reflectivity of the output coupler for a given cavity. In general, lowering the signal reflectivity results in higher signal pulse energies. This behavior was predicted in [20]. The maximum signal pulse energies were experimentally found to be 15, 20, and 26 μJ for signal reflectivities of 95, 90 and 85%, respectively. Increasing the signal reflectivity of the output mirror not only reduces the pulse energy, but also may lead to satellite pulses accompanying the signal pulse, as shown in Fig.3-6. Therefore, the intracavity OPO can be improved by optimization of the signal reflectivity of the output mirror and by variation of the pulse repetition rate.

3.3 Conclusions

Operation of a singly resonant pulsed KTP intracavity OPO pumped by an AO Q-switched Nd:YVO₄ laser has been demonstrated. Using a type II non-critically phase-matched x-cut KTP crystal, eye-safe signal radiation at 1573 nm was generated in a plane-parallel to the intracavity OPO resonator. It was found that the maximum pulse energy may saturate beyond a given above-threshold intracavity OPO factor, but increasing the signal reflectivity of the output coupler can efficiently increases the average output power. The conversion efficiency for the average power is up to 10.6% from pump diode input to OPO signal output. The effective cavity dump of intracavity OPO leads to a relatively short signal pulse width for repetition rates from 10 to 80 kHz. As a consequence, the peak power for signal output can be up to several kilowatts

for the entire frequency range. The compact size and high efficiency of the present laser make it an attractive source for practical applications.



References

- [1] L.R. Marshall, A.D. Hays, J. Kasinski, R. Burnham: Proc. SPIE 1419,141 (1991)
- [2] E.O. Amman, J.M. Yarborough, M.K. Oshman, P.C.Montgomery: Appl.Phys. Lett. 16, 309 (1970)
- [3] M.K. Oshman S.E. Harris: IEEE J. Quantum Electron. 4, 491(1968)
- [4] J. Falk, J.M. Yarborough, E.O. Amman: IEEE J. Quantum Electron. 7,359 (1971)
- [5] R. Lavi, A. Englander, R. Lallouz: Opt. Lett. 21, 800 (1996)
- [6] A.R. Geiger, H. Hemmati, W.H. Farr, N.S. Prasad: Opt. Lett. 21, 201(1996)
- [7] Y. Yashkir, H.M. van Driel: Appl. Opt. 38, 2554 (1999)
- [8] L.R. Marshall, J. Kasinski, R. Burnham: Opt. Lett. 16, 1680 (1991)
- [9] L.R. Marshall, A. Kaz: J. Opt. Soc. Am. B 10, 1730 (1993)
- [10] G. Xiao, M. Bass, M. Acharekar: IEEE J. Quantum Electron. 34, 2241(1998)
- [11] R. Dabu, C. Fenic, A. Stratan: Appl. Opt. 40, 4334 (2001)
- [12] A. Dubois, S. Victori, T. L'epine, P. Georges, A. Brun: Appl. Phys. B 67,181 (1998)
- [13] A. Agnesi, S. Dell'Acqua, G. Reali: Appl. Phys. B 70, 751 (2000)
- [14] R.S. Conroy, C.F. Rae, G.J. Friel, M.H. Dunn, B.D. Sinclair: Opt. Lett.23, 1348 (1998)
- [15] J.J. Degnan: Surv. Geophys. 22, 431 (2001)
- [16] Y.F. Chen: Opt. Lett. 24, 1032 (1999)
- [17] J.J. Zayhowski, A. Mooradian: Opt. Lett. 14, 1989 (1989)
- [18] G.J. Dixon, L.S. Lingvay, R.H. Jarman: Proc. SPIE 1104, 107(1989)
- [19] Y.F. Chen, T.M. Huang, C.F. Kao, C.L.Wang, S.C.Wang: IEEE J. Quantum Electron. 33, 1424 (1997)
- [20] T. Debuisschert, J. Raffy, J.P. Pocholle, M. Papuchon: J. Opt. Soc. Am. B 13, 1569 (1996)

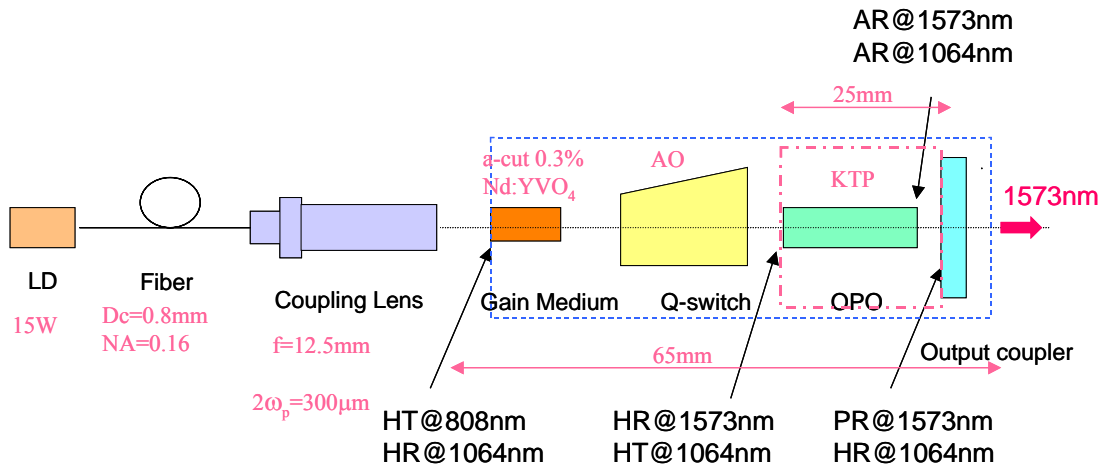


Fig.3-1 Schematic of the intracavity OPO pumped by a cw diode-pumped AO Q-switched Nd:YVO₄ laser

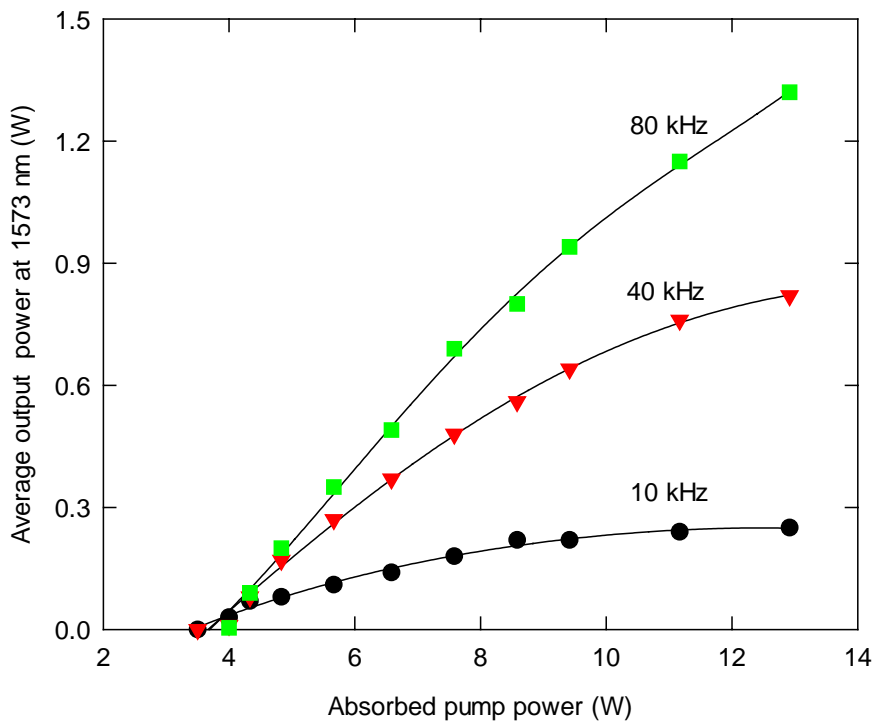


Fig.3-2 The average output power at 1573 nm versus the absorbed pump power for several pulse repetition rates

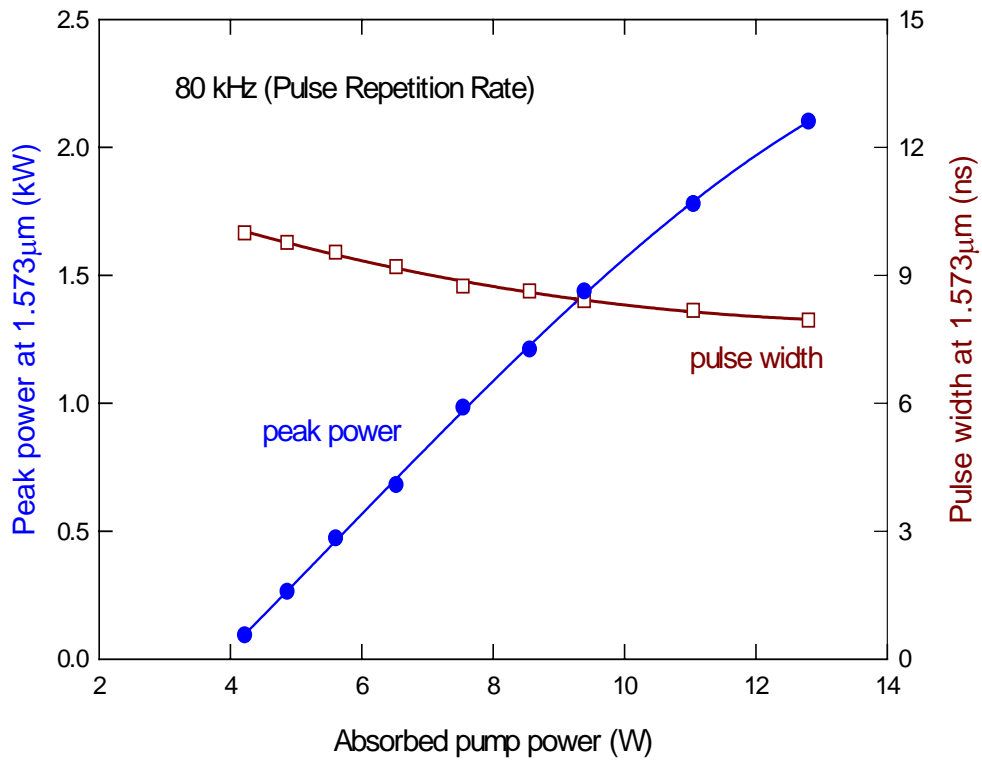


Fig.3-3 The peak power and pulse width at 1573 nm versus the absorbed pump power at a pulse repetition rate of 80 kHz

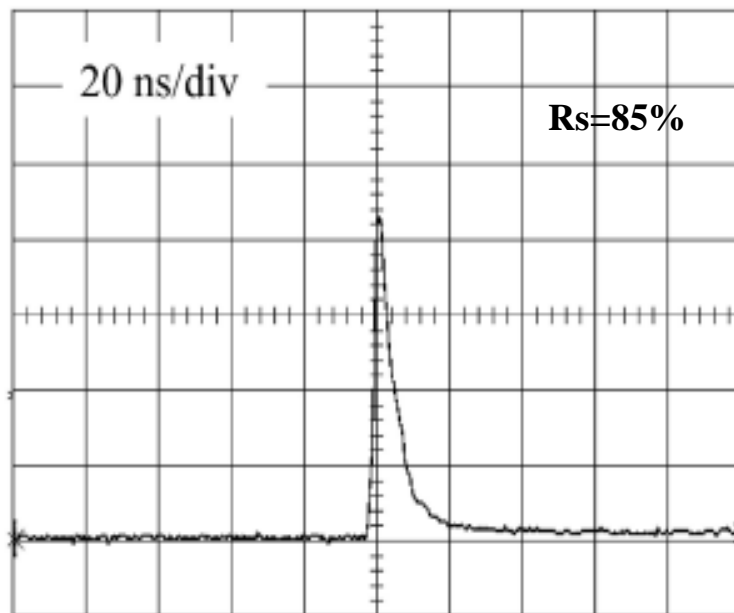


Fig.3-4 A typical pulse-shape at 1573 nm for a signal reflectivity of 85% on the output coupler

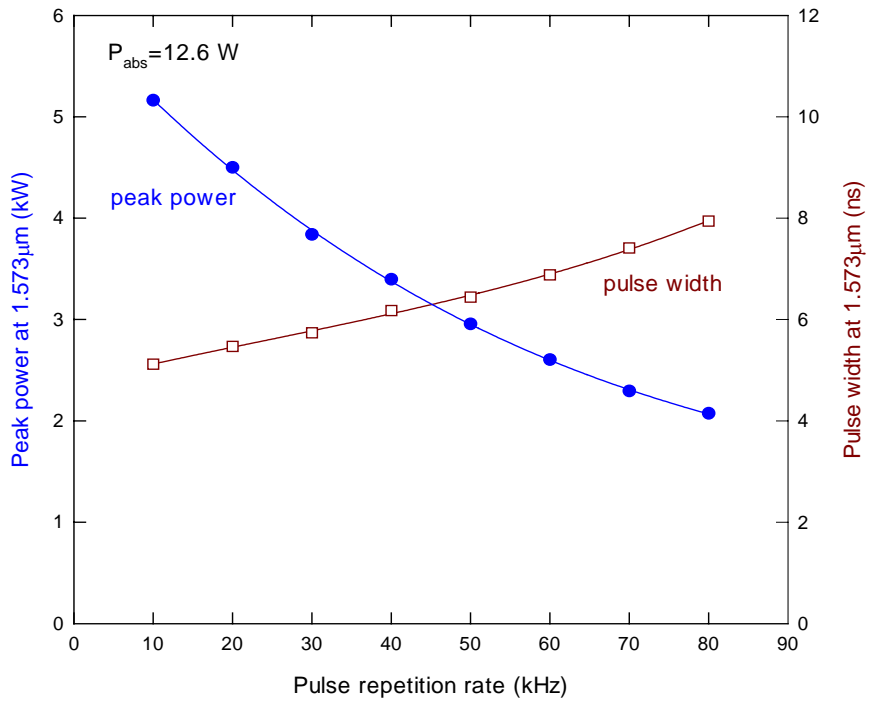
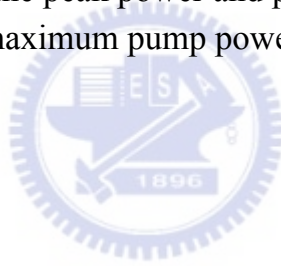
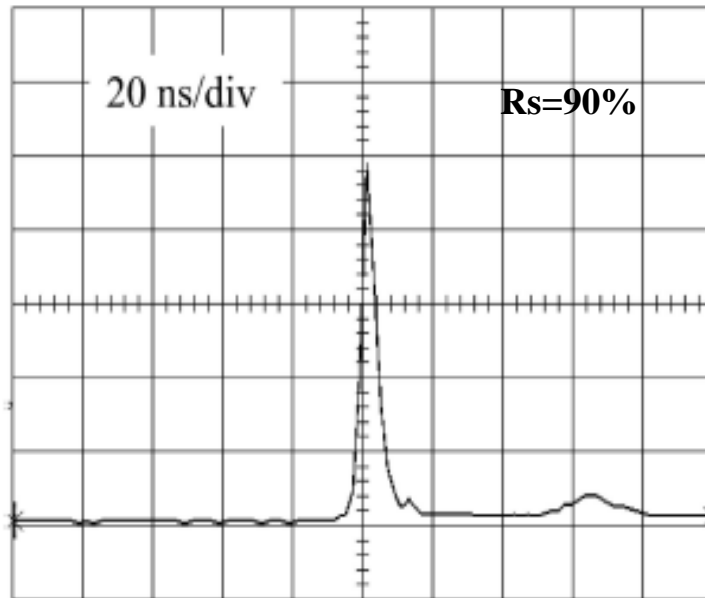


Fig.3-5 The dependence of the peak power and pulse width at 1573 nm on the pulse repetition rate at the maximum pump power of 12.6W



(a)



(b)

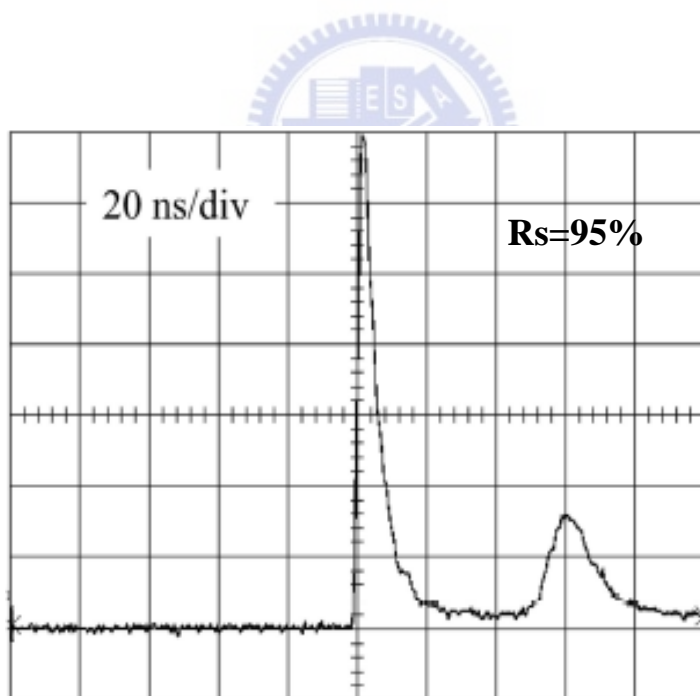


Fig.3-6 A typical pulse-shape at 1573 nm for signal reflectivities of a 90% and b 95% on the output coupler

Chapter 4 Output Optimization of a Diode-Pumped Actively Q-Switched

IOPO

4.1 Introduction

High-peak-power laser sources at wavelengths greater than $1.5 \mu\text{m}$ are vital for applications involving coherent laser radar, remote sensing and active imaging [1]. In this spectral range, radiation is mostly absorbed in the ocular fluid of the eye rather than in the retina. Eye safety is an important requirement for laser applications involving free space propagation. This need has stimulated much interest in intracavity optical parametric oscillators (OPOs). In comparison with extracavity configurations, intracavity OPOs take advantage of the high power level within the oscillator to allow a low threshold and high efficiency. Even though intracavity OPOs have been proposed for over 30 years [2–4], only recently have their merits been noted by the availability of high-damage-threshold non-linear crystals and diode-pumped Nd-doped lasers [1, 5–7]. Several crystals belonging to the potassium titanyl phosphate (KTP) family, when pumped by Nd-doped laser pumps around 1050–1070 nm, generate signal wavelengths around $1.55 \mu\text{m}$ [8–11]. The conventional intracavity OPOs in which flash lamps or quasi-cw diodes are used as the pump sources typically restrict operations to low repetition rates, less than 1 kHz [12, 13]. Although a compact diode-pumped Q-switched intracavity OPO has been demonstrated at a frequency repetition rate from 1 to 20 kHz, the overall average power is less than 60mW[14].

Recently, we demonstrated 1.33W of 1573-nm output from an intracavity OPO based on a non-critically phase-matched KTP pumped by a diode-pumped acousto-optically (AO) Q-switched Nd : YVO₄ laser operating at 80 kHz [15]. In this work, we experimentally study the output optimization of a high-repetition-rate diode-pumped Q-switched intracavity optical parametric oscillator at $1.57 \mu\text{m}$. Experimental results reveal that the output reflectivity for the maximum conversion

efficiency is in the range 85%–90%, whereas the highest peak power can be obtained with the output reflectivity around 60%–70%. Numerical analysis is performed to confirm the experimental results.

4.2 Experimental Setup

A schematic of the actively Q-switched intracavity OPO laser is shown in Fig.4-1. The active medium was an a-cut 0.3-at%. Nd^{3+} , 7-mm-long $\text{Nd}^{3+}:\text{YVO}_4$ crystal. A $\text{Nd}^{3+}:\text{YVO}_4$ crystal of low doping concentration was used to avoid thermally induced fracture [16]. Both sides of the laser crystal were coated for antireflection at 1064 nm ($R < 0.2\%$). The pump source was a 15-W 809-nm fiber-coupled laser diode with a core diameter of 0.8-mm and a numerical aperture of 0.16. A focusing lens with 12.5-mm focal length and 85% coupling efficiency was used to re-image the pump beam into the laser crystal. The waist radius of the pump beam was around 0.36mm. The input mirror, M1, was a 1-m radius of-curvature concave mirror with antireflection coating at the diode wavelength on the entrance face ($R < 0.2\%$), high-reflection coating at the lasing wavelength ($R > 99.8\%$) and high-transmission coating at the diode wavelength on the other surface ($T > 95\%$). The output coupler had a dichroic coating that was highly reflective at 1064 nm ($R > 99.8\%$) and partially reflective at 1573 nm. Several output couplers with different reflectivities ($50\% \leq R_s \leq 95\%$) at 1573 nm were used in the experiment to study the output optimization. The 10-mm-long AO Q-switcher (NEOS) was antireflection coated at 1064 nm on both faces and was driven at a 80MHz center frequency with 3.0W of rf power. To avoid damage to the intracavity optical components, the Q-switcher was operated above 10 kHz. The OPO cavity was formed by a coated KTP crystal and an output coupler. The 20-mm-long KTP crystal was used in type-II non-critical phase-matching configuration along the x-axis ($\theta = 90^\circ$ and $\varphi = 0^\circ$) to have both a maximum effective non-linear coefficient and no walk-off between the pump, signal and idler beams. One surface of the KTP crystal was coated to have high reflectivity at the signal wavelength of 1573 nm ($R > 99.8\%$) and high transmission at the pump wavelength of 1064 nm ($T > 95\%$). The other face of the KTP crystal was antireflection coated at 1573 nm and 1064 nm. Both the

Nd:YVO₄ and KTP crystals were wrapped with indium foil and mounted in a water-cooled copper block. The water temperature was maintained at 25°C. The overall Nd:YVO₄ laser cavity length was 55 mm and the OPO cavity length was 23 mm.

4.3 Result and Discussion

Fig.4-2 shows the average output power at 1573 nm as a function of the repetition for different output couplers at an absorbed pump power of 12.6W. The radius of the OPO beam was estimated to be around 0.3mm. Over the entire frequency range, the beam quality M^2 factor was found to be less than 1.3. Basically, increasing the pulse repetition rate can efficiently increase the average output power at 1573 nm, except that the OPO reflectivity is too low ($R_s = 50\%$). It can be also seen that a higher output coupler reflectivity (85% R_s 90%), on average, leads to higher conversion efficiency. However, if the OPO output reflectivity is too high, the stored energy is not fully extracted in a single output pulse. Since the remaining energy is sufficient to evolve the pump field, the OPO threshold can be reached again and a second signal pulse is produced. As shown in Fig.4-3a and b, a train of OPO pulses is usually produced for higher values of R_s , whereas a single pulse can be generated with a lower output reflectivity. In addition, the pulse width was found to be generally less than 5 ns. The short pulse width comes from the effective cavity dump of the intracavity OPO. Therefore, if high peak power is preferred, the OPO output reflectivity needs to be chosen to maximize the conversion in a single pulse.

We have employed the rate equation model developed by Debuisschert et al. [17] to confirm the consequent experimental results. Since the present IOPO is resonant only on the signal, the evolution equation of the idler field can be suppressed. With this adiabatic elimination, the rate equations for the four-level Q-switched laser with IOPO are given by:

$$\frac{dn}{dt} = -c\sigma\phi_p n \quad (4-1)$$

$$\frac{d\phi_P}{dt} = \frac{l_{cr}}{l_{ca}} c \sigma n (\phi_P + \Delta\phi_P) - \frac{l_{nl}}{l_{ca}} \sigma_{OPO} \phi_S \phi_P - \frac{\phi_P}{t_{rp}} \left[\ln\left(\frac{1}{R}\right) + L \right] \quad (4-2)$$

$$\frac{d\phi_S}{dt} = c \sigma_{OPO} \phi_P (\phi_S + \Delta\phi_S) - \frac{\phi_S}{t_{rs}} \left[\ln\left(\frac{1}{R_S}\right) + L_S \right] \quad (4-3)$$

where n is the inversion population density of the gain medium, c is the speed of light, ϕ_P is the pump photon density, ϕ_S is the signal photon density, l_{ca} is the optical length of the laser cavity, σ is the stimulated emission cross section of the gain medium, t_{rp} is the round-trip time in the laser cavity, l_{cr} is the length of the gain medium, l_{nl} is the length of the non-linear crystal, $\Delta\phi_P$ is the spontaneous emission intensity, L is the round-trip pump wave intensity loss in the laser cavity, R is the global reflectivity of the laser cavity mirrors, t_{rs} is the round-trip time in the OPO resonator, σ_{OPO} is the effective OPO conversion cross section, $\Delta\phi_S$ is the noise signal intensity, L_S is the round-trip signal wave intensity loss in the OPO cavity and R_S is the output reflectivity of the OPO mirror.

Equations(4-1)–(4-3) are essentially identical to those used by Debuisschert et al. [17], except that the effective OPO cross section is used to describe the conversion rate. The effective OPO cross section, σ_{OPO} , can be derived from the parametric gain coefficient for small gains of the single resonator oscillator:

$$2\sigma_{OPO} l_{nl} = \frac{8\omega_1\omega_2 d_{eff}^2 l_{nl}^2}{n_1 n_2 n_3 \varepsilon_0 c^2} \frac{\frac{2}{3}}{\frac{2}{2} + \frac{2}{3}} \quad (4-4)$$

where ω_1, ω_2 are the idler and signal frequencies, respectively; n_1, n_2, n_3 are the refractive indices at the idler, signal and pump wavelengths, respectively; d_{eff} is the effective non-linear coefficient; ε_0 is the vacuum permittivity; and $\frac{2}{2}$ and $\frac{2}{3}$ are the mode sizes for the signal and laser waves, respectively.

Fig.4-4a and b depicts the calculated temporal profiles corresponding to the expe-

perimental results shown in Fig. 4-3a and b, respectively. The good agreement between experimental and numerical results indicates that the theoretical model is successful in predicting the production of several signal pulses. Fig.4-5 shows the experimental and theoretical results for the average output power versus the OPO output reflectivity at a repetition rate of 80-kHz and an absorbed pump power of 12.6 W.

It can be seen that the theoretical calculations agree quite well with the experimental data. The optimum output coupler for the maximum average power is found to be approximately $R_s = 85\%$. With the optimum output coupler, the conversion efficiency from the diode laser input power to OPO signal output power is up to 15%. Although the highest conversion efficiency was obtained with an output coupler of $R_s = 85\%$, the peak power was a maximum with an output coupler of $R_s = 60\%–70\%$, as shown in Fig.4-6. It can be seen that with an output coupler of $R_s = 60\%–70\%$, the peak power can amount to 3–4 kW at a pulse repetition rate of 80 kHz and an absorbed pump power of 12.6W. From the experimental results shown in Figs. 4-5 and 4-6, an output coupler of $R_s = 80\%$ is found to be a better choice for the tradeoff between the average power and the peak power.

Finally, it is worthwhile to mention that the pulse repetition rates in the present experiment (> 20 kHz) are considerably higher than those in conventional Q-switched lasers (< 1 kHz). On the whole, the optimum output reflectivity increases with increasing pulse repetition rate; this is the reason why the optimum output reflectivity is significantly higher than that for conventional output couplers in Q-switched lasers.

4.4 Conclusions

We have studied the output optimization of a high-repetition-rate diode-pumped Q-switched intracavity optical parametric oscillator at 1573 nm with a type-II non-critically phase-matched x-cut KTP crystal. Numerical calculations have also been performed to confirm the experimental results. It was found that the maximum conversion efficiency can be obtained with an output coupler of 85%–90% at the cost of peak power. If high peak power is desired, the output reflectivity needs to be around 60%–70%.

References

- [1] R.C. Stoneman, L. Esterowitz: In: Proc. Conf. Adv. Solid State Lasers, Salt Lake City, Utah (Optical Society of America, Washington DC 1990) pp. 176–178, paper WC5-2; L.R. Marshall, A.D. Hays, J. Kasinski, R. Burnham: Proc. SPIE 1419, 141 (1991)
- [2] E.O. Amman, J.M. Yarborough, M.K. Oshman, P.C. Montgomery: Appl. Phys. Lett. 16, 309 (1970)
- [3] M.K. Oshman, S.E. Harris: IEEE J. Quantum Electron. QE-4, 491(1968)
- [4] J. Falk, J.M. Yarborough, E.O. Amman: IEEE J. Quantum Electron. QE-7, 359 (1971)
- [5] R. Lavi, A. Englander, R. Lallouz: Opt. Lett. 21, 800 (1996)
- [6] A.R. Geiger, H. Hemmati, W.H. Farr, N.S. Prasad: Opt. Lett. 21, 201(1996)
- [7] Y. Yashkir, H.M. van Driel: Appl. Opt. 38, 2554 (1999)
- [8] L.R. Marshall, J. Kasinski, R. Burnham: Opt. Lett. 16, 1680 (1991)
- [9] L.R. Marshall, A. Kaz: J. Opt. Soc. Am. B 10, 1730, 10 (1993)
- [10] G. Xiao, M. Bass, M. Acharekar: IEEE J. Quantum Electron. QE-34, 2241 (1998)
- [11] R. Dabu, C. Fenic, A. Stratan: Appl. Opt. 40, 4334 (2001)
- [12] A. Dubois, S. Victori, T. L'epine, P. Georges, A. Brun: Appl. Phys. B 67, 181 (1998)
- [13] A. Agnesi, S. Dell'Acqua, G. Reali: Appl. Phys. B 70, 751 (2000)
- [14] R.S. Conroy, C.F. Rae, G.J. Friel, M.H. Dunn, B.D. Sinclair: Opt. Lett. 23, 1348 (1998)
- [15] Y.F. Chen: IEEE J. Quantum Electron. QE-35, 234 (1999)
- [16] Y.F. Chen, S.W. Chen, S.W. Tsai, Y.P. Lan: Appl. Phys. B 76, 263 (2003)
- [17] T. Debuisschert, J. Raffy, J.P. Pocholle, M. Papuchon: J. Opt. Soc. Am. B 13, 1569 (1996)

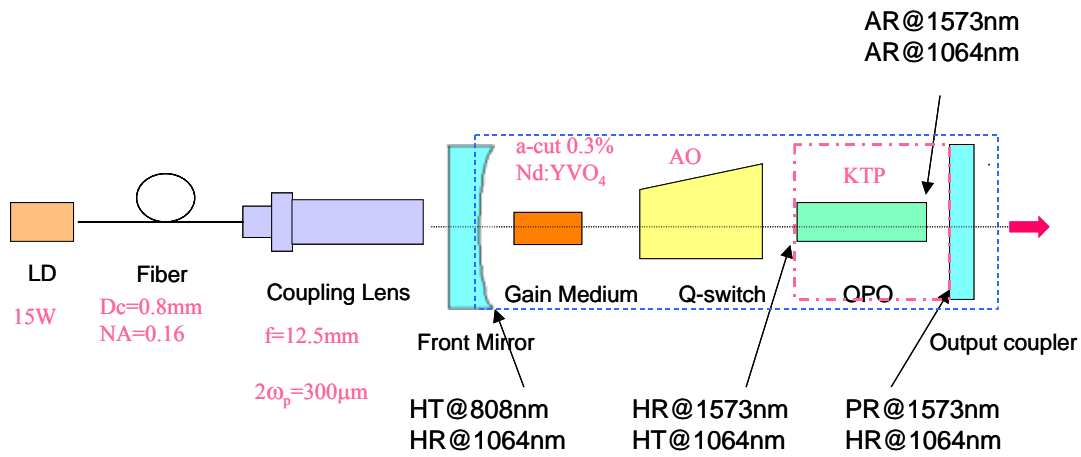


Fig.4-1 Schematic of the actively Q-switched intracavity OPO laser

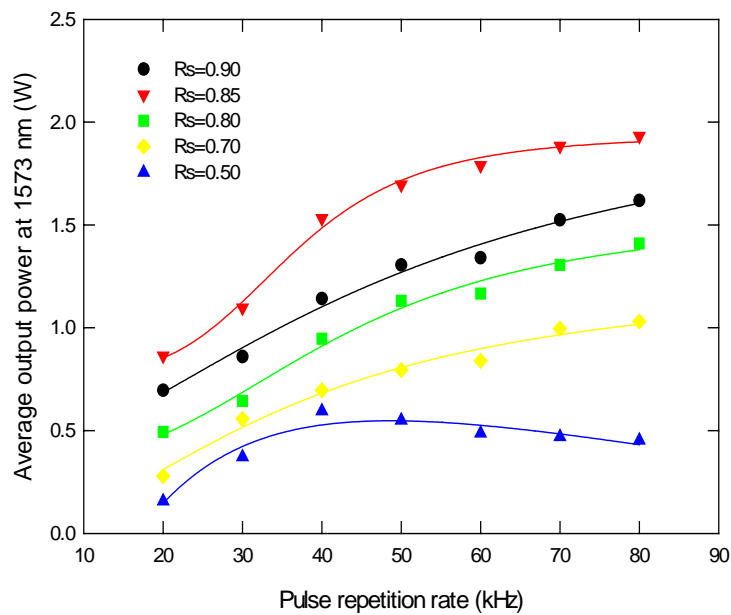
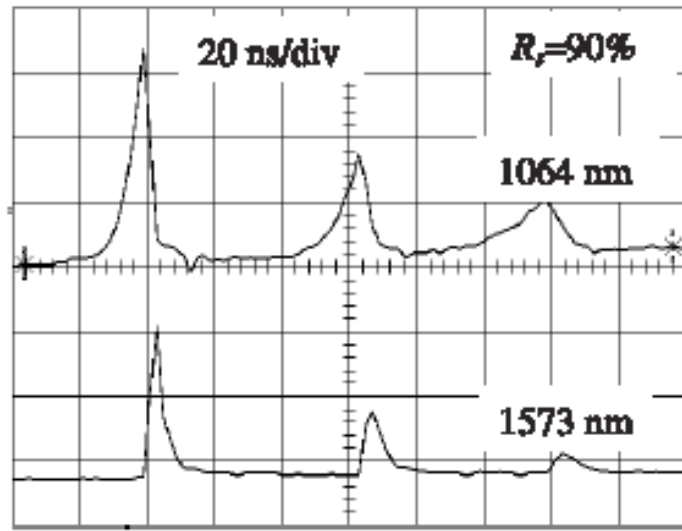


Fig.4-2 The average output power at 1573 nm as a function of the repetition for different output couplers at an absorbed pump power of 12.6W

(a)



(b)

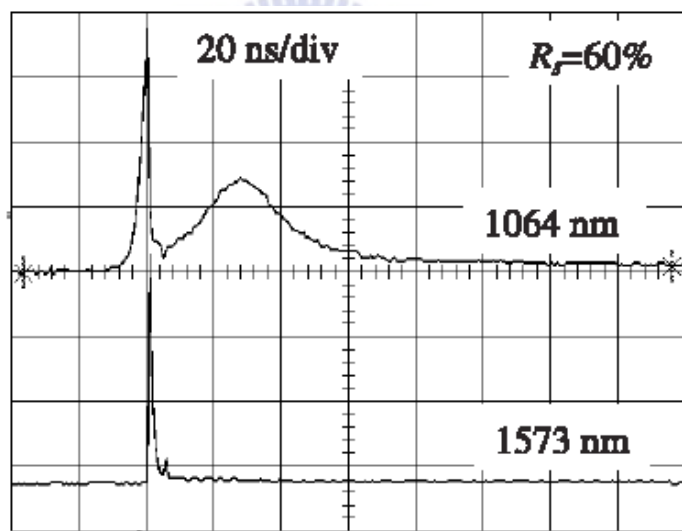


Fig.4-3 Oscilloscope traces showing a train of pump and signal pulses when $R_s = 90\%$ (a), and a single pulse for pump and signal fields when $R_s = 60\%$ (b). Both results were measured at a pulse repetition rate of 80 kHz and an absorbed pump power of 12.6W

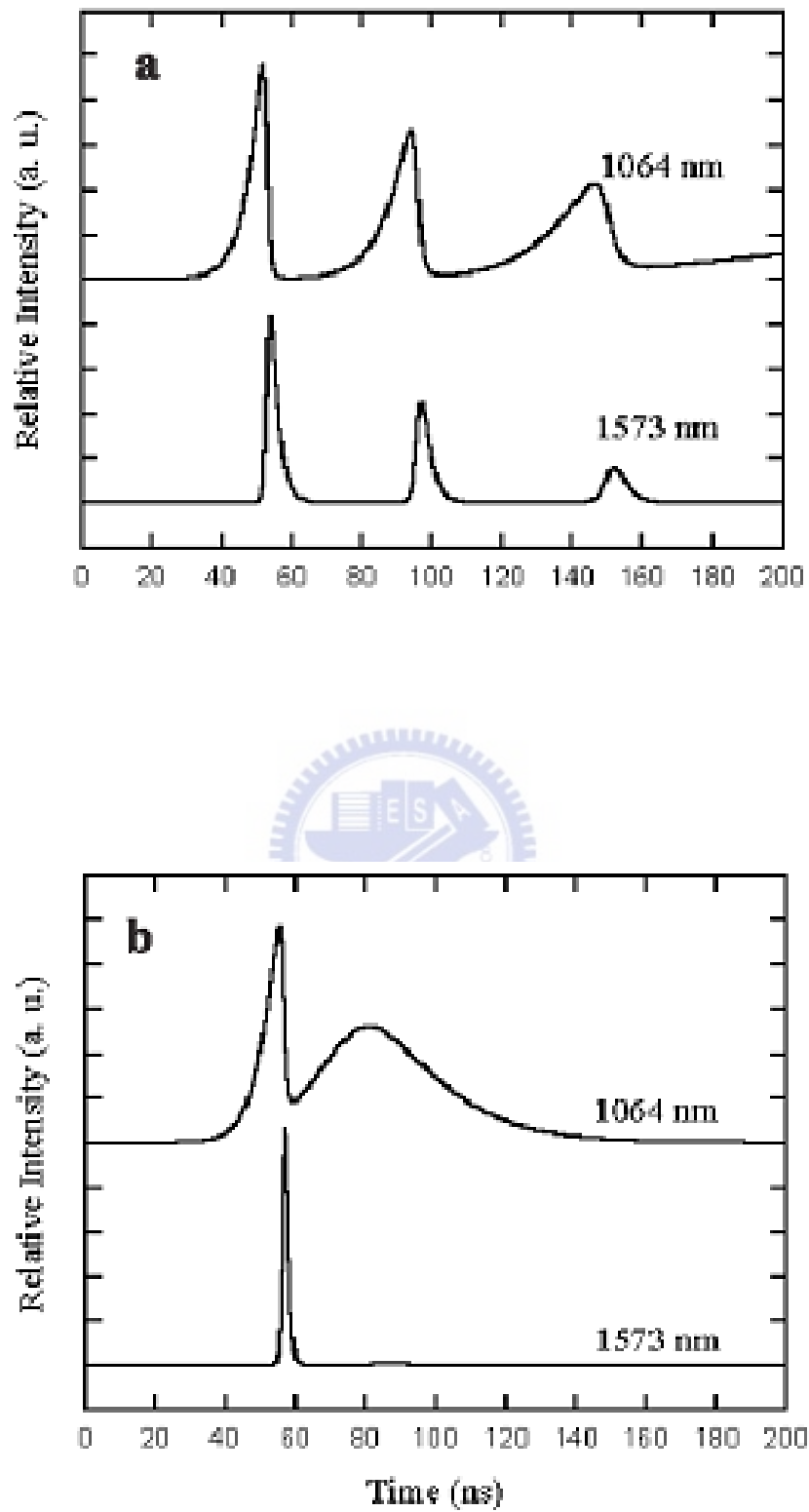


Fig.4-4 The calculated temporal profiles corresponding to the experimental results shown in Fig.3a and b, respectively

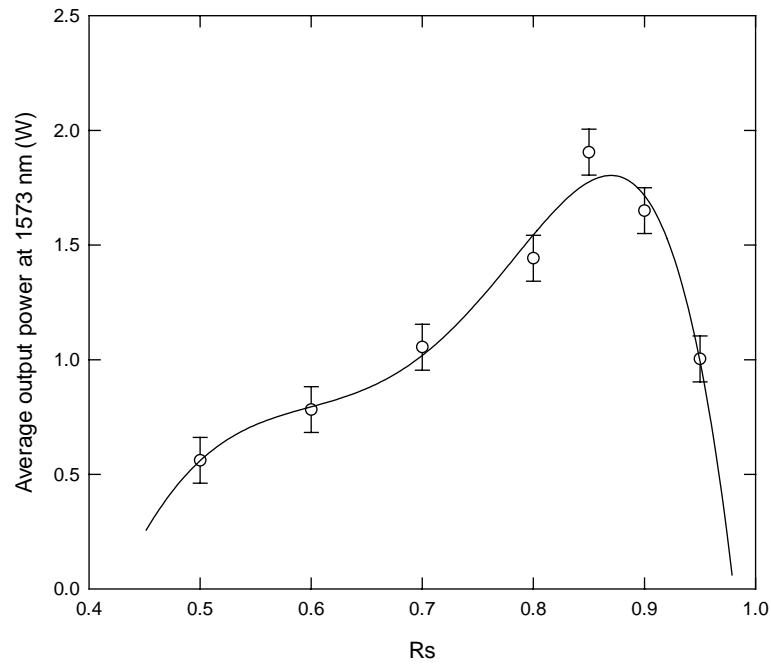


Fig.4-5 Experimental and theoretical results for the average output power versus the OPO output reflectivity at a repetition rate of 80 kHz and an absorbed pump power of 12.6W

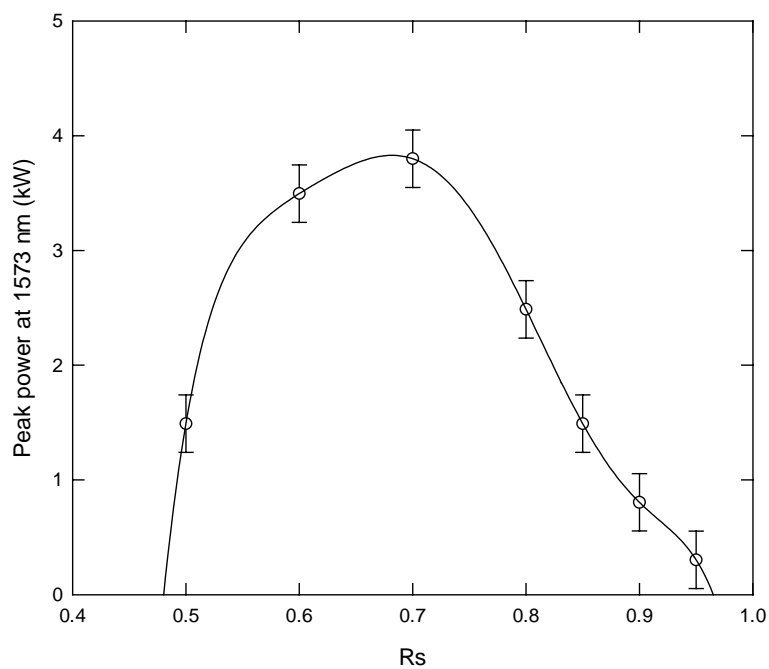


Fig.4-6 Experimental and theoretical results for the output peak power versus the OPO output reflectivity at a repetition rate of 80 kHz and an absorbed pump power of 12.6W

Chapter 5 Intracavity OPO with a Passively Q-Switched Nd:YVO₄ Laser

5.1 Introduction

Compact pulsed lasers with emission at the eyesafe wavelength region (1.5–1.6 μm) are of great interest for many applications such as telemetry and range finders [1]. The need for high-peak-power eyesafe laser sources has stimulated much interest in intracavity optical parametric oscillators (OPO's). Although intracavity OPO's have been proposed for over 30 years [2–4], only recently have their merits been appreciated, with the advent of high-damage-threshold nonlinear crystals and diode-pumped Nd-doped lasers [1, 5–7]. Diode-pumped Q-switched microchip lasers are compact efficient solid-state lasers with a diffraction-limited output beam. Saturable-absorber Q-switching has the advantages of potentially lower cost and simplicity in fabrication and operation. In recent year, Cr⁴⁺ : YAG crystals have been successfully used as passive Q-switches for a variety of gain media such as Nd :YAG [8], Nd :YVO₄ [9–11], and Nd : GdVO₄ crystals [12], etc. Nd :YVO₄ and Nd : GdVO₄ crystals have several advantages over Nd :YAG crystals, including higher absorption cross section, wider absorption bandwidth, and a polarized output. The linearly polarized laser output is beneficial not only to non-linear wavelength conversion, but also to avoiding of undesired birefringent effects. It is, however, usually difficult to operate a diode pumped passively Q-switched Nd :YVO₄ and Nd : GdVO₄ lasers with Cr⁴⁺ :YAG saturable absorbers because of their large emission cross-sections. For good passive Q-switching, absorption saturation in the absorber must occur before gain saturation in the laser crystal (the second threshold condition) [13, 14]. Even though passively Q-switched Nd :YVO₄ and Nd : GdVO₄ lasers have been demonstrated [9–12], the output pulse energy and peak power are obviously lower than those of Nd :YAG laser. Therefore, so far the pumped sources for passively Q-switched intracavity OPO's are mostly composed of Nd :YAG and Cr⁴⁺ :YAG crystals. The relatively narrow absorption band of Nd :YAG crystal, however, sets stringent requirements on the spectrum of the pump diodes. In this work we report a compact, efficient scheme for

generating 1573-nm laser based on intracavity OPO of a diode pumped passively Q-switched Nd :YVO₄/Cr⁴⁺ :YAG laser. With an incident pump power of 2.5W, the compact intracavity OPO cavity, operating at 62.5 kHz, produces average powers at 1573 nm up to 255mW and peak powers higher than 1 kW.

5.2 Experimental Setup

Fig.5-1 is a schematic of the passively Q switched intracavity OPO laser. The novelty is that a saturable absorber Cr⁴⁺:YAG is coated as an output coupler of the OPO cavity and a nearly hemispherical cavity is used to enhance the performance of passive Q-switching. The active medium was an a-cut 1.0 at.% Nd³⁺, 2-mm-long Nd³⁺:YVO₄ crystal. Both sides of the laser crystal were coated for antireflection at 1064 nm (R<0.2%). The pump source was a 2.5-W 808-nm fiber-coupled laser diode with a core diameter of 200 μm and a numerical aperture of 0.16. Focusing lens with 12.5mm focal length and 95% coupling efficiency was used to re-image the pump beam into the laser crystal. The average pump-spot radius, ω_p , was around 150 μm. The input mirror was a 50 mm radius-of-curvature concave mirror with antireflection coating at the diode wavelength on the entrance face (R<0.2%), high-reflection coating at lasing wavelength (R>99.8%) and high-transmission coating at the diode wavelength on the other surface (T> 95%). Note that the laser crystal was placed very near (0.5 ~1mm) the input mirror. The OPO cavity was formed by a coated KTP crystal and a coated Cr⁴⁺:YAG crystal. The 20-mm-long KTP crystal was used in type II noncritical phase-matching configuration along the x axis ($\theta = 90^\circ$ and $\varphi = 0^\circ$) to have both a maximum effective nonlinear coefficient and no walkoff between the pump, signal, and idler beams [15-18]. The KTP crystal was coated to have high reflectivity at the signal wavelength of 1573 nm (R>99.8%) and high transmission at the pump wavelength of 1064 nm (T>95%). The other face of the KTP crystal was antireflection coated at 1573 nm and 1064 nm. The Cr⁴⁺ :YAG crystal has a thickness of 2mm with 80% initial transmission at 1064 nm. One side of the Cr⁴⁺ :YAG crystal was coated so that it was nominally highly reflecting at 1064 nm (R>99.8%) and partially reflecting at 1573 nm (R_s=80%). The remaining side was antireflection coated at 1064 and 1573 nm. The

overall Nd:YVO₄ laser cavity length was approximately 55 mm and the OPO cavity length was about 23mm.

5.3 Result and Discussion

The mode beam radii w_1 on the laser crystal and w_2 on the saturable absorber can be given by

$$w_1 = \sqrt{\frac{\lambda L_c}{\pi}} \sqrt{\frac{L_c}{R_c - L_c}}, \quad w_2 = \sqrt{\frac{\lambda L_c}{\pi}} \sqrt{\frac{R_c - L_c}{L_c}} \quad (5-1)$$

where λ is the lasing wavelength, L_c is the effective cavity length, and R_c is the radius of curvature of the input mirror. The effective cavity length is given by $L_c = L_c^* + l(1/n - 1) + l_{KTP}(1/n_{KTP} - 1)$, L_c^* is the cavity length, n is the refractive indices along the c axis of the Nd:YVO₄ crystal, l is the length of the Nd:YVO₄ crystal, l_{KTP} is the length of the KTP crystal, and n_{KTP} is the KTP refractive index for the output laser beam. For the present cavity length of $L_c^* = 55\text{mm}$, w_1 and w_2 can be calculated to be 225 μm and 71 μm , respectively.

With $w_1 = 225 \mu\text{m}$ and $w_p = 150 \mu\text{m}$, the ratio between the mode and pump area, $\alpha = (w_1/w_p)^2 = 2.25$, satisfies the design criterion of mode-matching optimization [19]. On the other hand, the ratio of the mode area in the gain medium and in the saturable absorber, $A/A_S = (w_1/w_2)^2 = 10$, satisfies the criterion for good passively Q-switching [13, 14].

Fig.5-2 shows the average output power and the pulse repetition rate at 1573 nm with respect to the absorbed pump power. For all pump powers the beam quality M^2 factor was found to be less than 1.3. The average output power reached 255mW, and the pulse repetition rate was 62.5 kHz at an incident pump power of 2.5W. The threshold power and the slope efficiency were 1.1W and 18.3%, respectively. The conversion efficient from diode laser input power to OPO signal output power was 10.2%. To the

best of our knowledge, this is highest efficiency for average power conversion reported to date.

The pulse temporal behavior at 1573 nm was recorded by a LeCroy 9362 digital oscilloscope (500MHz bandwidth) with a fast germanium photodiode. An oscilloscope trace of a train of the signal pulses is shown in the inset of Fig5- 2. The pulse-to-pulse amplitude fluctuation was found to be within $\pm 10\%$. Fig.5-3 shows typical temporal shapes for the laser and signal pulses. The relatively short signal pulse indicates that the OPO effectively cavity dumps the laser energy. Experimental results reveal that the signal pulse width decreases from 6.0 ns at threshold to 3.8 ns at 2.5W of incident pump power. Fig.5-4 depicts the peak power and the pulse energy at 1573 nm versus the absorbed pump power. It is seen that the pulse energy initially increases with pump power, and is almost saturated beyond 2 times the OPO threshold. The striking feature is that with the maximum pump power of 2.5W the signal peak power can exceed 1 kW at a pulse repetition rate of 62.5 kHz.

Finally, it is worthwhile to mention that the temporal characteristics of the present cavity highly depend on the laser alignment, pump spot size and mirror reflectivity. As shown in Fig.5-5, a train of laser and signal pulses is usually produced for a higher OPO reflectivity on the output coupler ($R_s = 90\%$). Under the normal mode-matching circumstances, the output optimization of the present cavity mainly consists in the design of the output reflectivity. Experimental results reveal that the maximum conversion efficiency can be obtained with an output coupler of 85 - 90% at the sacrifice of peak power. If the high peak power is desired, the output reflectivity needs to be around 60-70%.

5.4 Summary

In summary, operation of a singly resonant pulsed KTP intracavity OPO pumped by a diode-pumped passively Q-switched Nd :YVO₄/Cr⁴⁺ :YAG laser has been demonstrated. A saturable absorber Cr⁴⁺ : YAG was coated as an output coupler of the OPO cavity to constitute a realistic, inexpensive source of eye-safe nanosecond laser. The low threshold power permits the use of a relatively low-power laser diode (2.5W).

The conversion efficiency for the average power is up to 10.2% from pump diode input to OPO signal output. The effective cavity dump of intracavity OPO leads to the relatively short signal pulse width with high repetition rates. As a consequence, the signal peak power can exceed 1 kW with a pulse repetition rate of 62.5 kHz at an incident pump power of 2.5W.



References

- [1] L.R. Marshall, A.D. Hays, J. Kasinski, R. Burnham: Proc. SPIE 1419, 141 (1991)
- [2] E.O. Amman, J.M. Yarborough, M.K. Oshman, P.C.Montgomery: Appl. Phys. Lett. 16, 309 (1970)
- [3] M.K. Oshman, S.E. Harris: IEEE J. Quantum Electron. QE-4, 491 (1968)
- [4] J. Falk, J.M. Yarborough, E.O. Amman: IEEE J. Quantum Electron. QE-7, 359 (1971)
- [5] R. Lavi, A. Englander, R. Lallouz: Opt. Lett. 21, 800 (1996)
- [6] A.R. Geiger, H. Hemmati, W.H. Farr, N.S. Prasad: Opt. Lett. 21, 201 (1996)
- [7] Y. Yashkir, H.M. van Driel: Appl. Opt. 38, 2554 (1999)
- [8] J.J. Zayhowski, C. Dill III: Opt. Lett. 19, 1427 (1994)
- [9] Y. Bai, N. Wu, J. Zhang, J. Li, S. Li, J. Xu, P. Deng: Appl. Opt. 36, 2468(1997)
- [10] Y.F. Chen, T.M. Huang, C.L.Wang, Electron. Lett. 33, 1880 (1997)
- [11] Y.F. Chen: IEEE Photon. Technol. Lett. 19, 1427 (1997)
- [12] C. Li, J. Song, D. Shen, N.S. Kim, J. Lu, K. Ueda: Appl. Phys. B 70, 471(2000)
- [13] A.E. Siegman: Laser (University Science, Mill Valley, California 1986) p. 1024 and p. 1012
- [14] Y.F. Chen, S.W. Tsai, S.C. Wang: Opt. Lett. 25, 1442 (2000)
- [15] L.R. Marshall, J. Kasinski, R. Burnham: Opt. Lett. 16, 1680 (1991)
- [16] L.R. Marshall, A. Kaz: J. Opt. Soc. Am. B 10, 1730 (1993)
- [17] G. Xiao, M. Bass, M. Acharekar: IEEE J. Quantum Electron. QE-34, 2241 (1998)
- [18] R. Dabu, C. Fenic, A. Stratan: Appl. Opt. 40, 4334 (2001)
- [19] P. Laporta, M. Brussard: IEEE J. Quantum Electron. QE-27, 2319(1991)

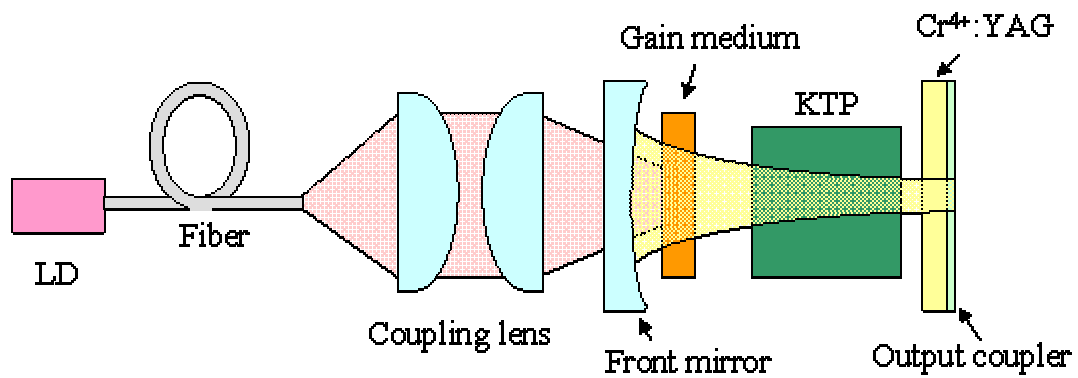


Fig.5-1 Schematic of the intracavity OPO pumped by a diode-pumped passively Q-switched Nd : YVO₄/Cr⁴⁺ : YAG laser

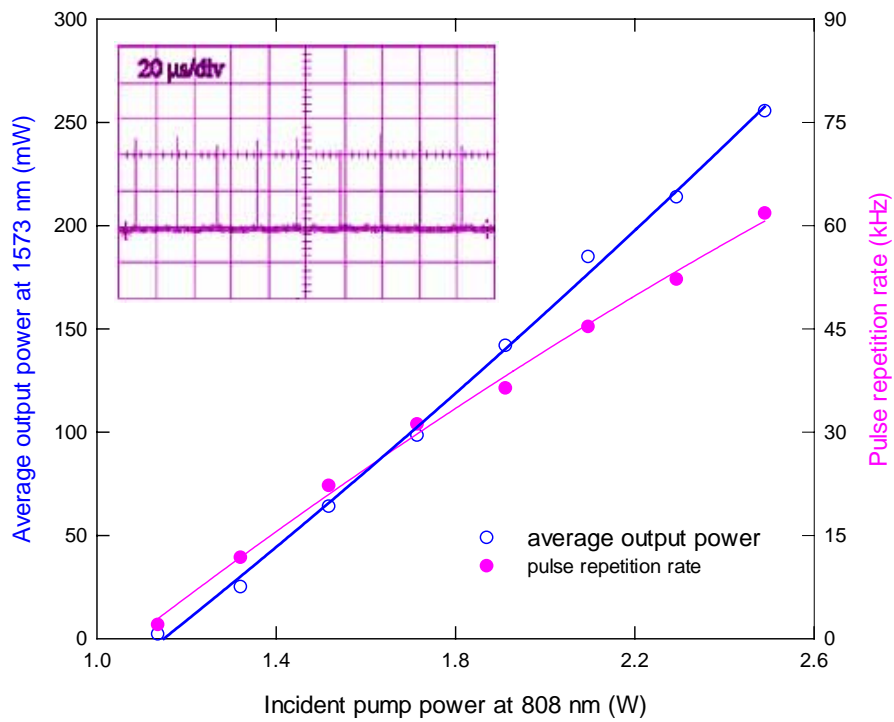


Fig.5-2 Dependence of the average output power and the pulse repetition rate at 1573 nm on the absorbed pump power. An oscilloscope trace of a train of the signal pulses is shown in the inset

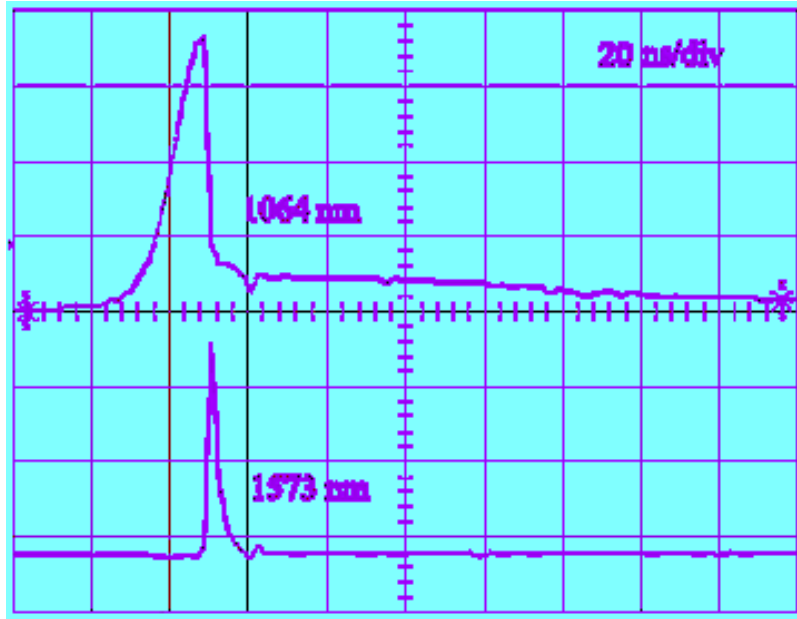


Fig.5-3 Typical temporal shapes for the laser and signal pulses with a signal reflectivity of 80% on the output coupler

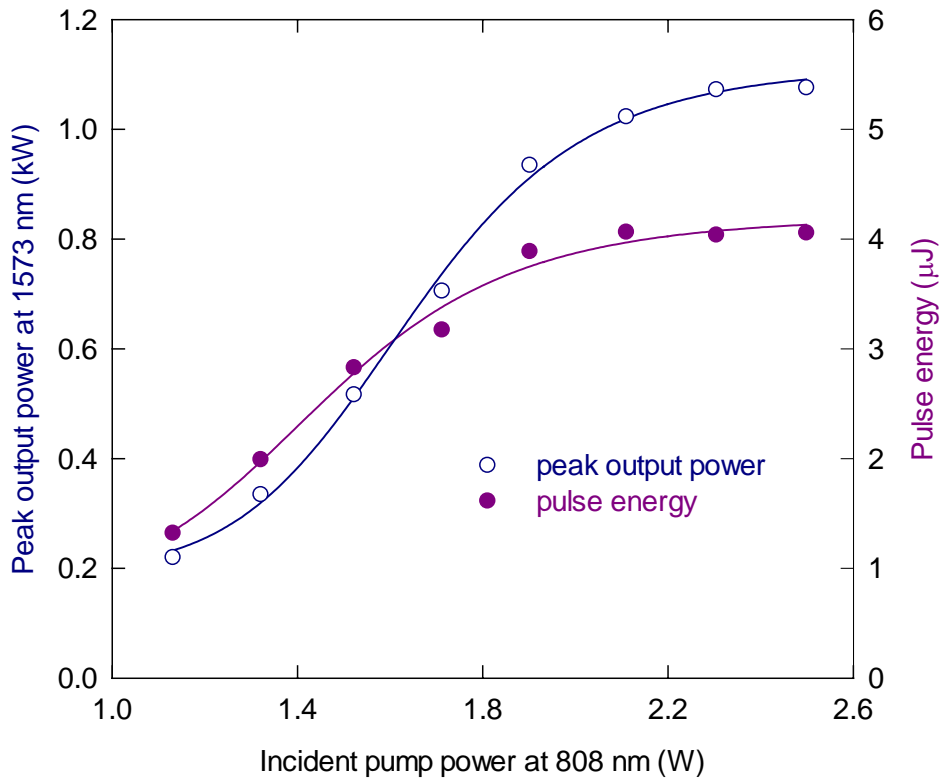


Fig.5-4 Dependence of the peak power and the pulse energy at 1573 nm on the absorbed pump power

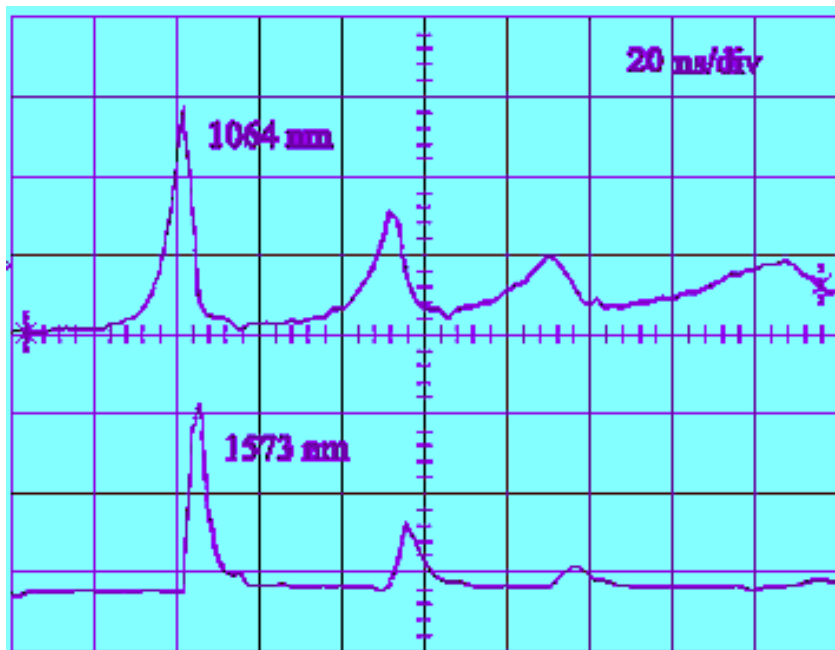
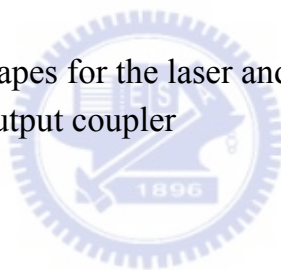


Fig.5-5 Typical temporal shapes for the laser and signal pulses with a signal reflectivity of 90% on the output coupler



Chapter 6 Output Optimization of Diode-pumped Passively Q-Switched

Nd:YVO₄/KTP/Cr⁴⁺:YAG Laser

6.1 Introduction

Nanosecond pulsed lasers at the eye-safe wavelength region (1.5–1.6 μm) are indispensable to applications such as telemetry and range finders [1]. Laser emission at this spectral range has been reported from several gain materials including Co:MgF₂ [2], Ni:MgF₂ [3], Cr⁴⁺:YAG [4,5], Er³⁺:YLiF₄ [6], Er³⁺:KY(WO₄)₂ [7], Er³⁺:YVO₄ [8], Yb³⁺:Tm³⁺:YLiF₄ [9] and Er:Yb:glass [10]. Pulsed operation near 1.55 μm has been achieved with passive Q-switching by use of Co²⁺:LaMg Al₁₁O₁₉ [11], Er:Ca₅(PO₄)₃F [12], U⁴⁺:CaF₂ [13], U⁴⁺:SrF₂ [14], Co²⁺:ZnSe [15], Cr²⁺:ZnSe [16] or a semiconductor saturable absorber mirror (SESAM) [17]. Another approach for high-peak-power eye-safe laser sources is based on intracavity optical parametric oscillators (OPOs) [18]. Recently, there has been a resurgence of interest in intracavity OPOs, as their merits have been appreciated with the advent of high-damage-threshold nonlinear crystals and diode-pumped Nd-doped lasers [19–21]. Diode-pumped Q-switched Nd-doped lasers are compact efficient solid-state lasers. In recent year, Cr⁴⁺:YAG crystals have been successfully used as passive Q-switches for a variety of gain media such as Nd:YAG [22], Nd:YVO₄ [23], and Nd:GdVO₄ crystals [24], etc. Even though passively Q-switched Nd:YVO₄ and Nd:GdVO₄ lasers have been demonstrated, their large emission cross-sections lead to the output pulse energy and peak power to be obviously lower than those of Nd:YAG laser. Therefore, so far the pumped sources for passively Q-switched intracavity OPOs are mostly composed of Nd:YAG and Cr⁴⁺:YAG crystals. The relatively narrow absorption band of Nd:YAG crystal, however, sets stringent requirements on the spectrum of the pump diodes. Recently, we demonstrated a compact efficient eye-safe OPO to produce 255 mW at 1573 nm by using a nearly hemispherical cavity [25]. In this work we consider the thermal lensing effects to scale up the average output power and peak power at 1573 nm based on a diode-pumped

passively Q-switched Nd:YVO₄/KTP/Cr⁴⁺:YAG intracavity OPO. The design of the mode-to-pump size ratio is one of the critical issues for a high-power end-pumped laser [26]. The theoretical analysis indicates that the optimum mode-to-pump size ratio for high pump power can be nearly satisfied by controlling the pump size in the previous cavity configuration. With an incident pump power of 14.5 W, the compact intracavity OPO cavity, operating at 58.5 kHz, produces average powers at 1573 nm up to 1.56 W and peak powers higher than 5 kW.

6.2 Experimental Setup

Fig.6-1 is a schematic of the passively Q-switched intracavity OPO laser. Here a saturable absorber Cr⁴⁺:YAG is coated as an output coupler of the OPO cavity and a nearly hemispherical cavity is used to enhance the performance of passive Q-switching. The active medium was an a-cut 0.5 at.% Nd³⁺, 7-mm long Nd:YVO₄ crystal. Both sides of the laser crystal were coated for antireflection at 1064 nm ($R < 0.2\%$). A Nd:YVO₄ crystal with low doping concentration was used to avoid the thermally induced fracture [27]. The laser crystal was wrapped with indium foil and mounted in a water-cooled copper block. The water temperature was maintained at 25 °C. The pump source was a 16-W 808-nm fiber-coupled laser diode with a core diameter of 800 μm and a numerical aperture of 0.2. Focusing lens with 12.5 mm focal length and 92% coupling efficiency was used to re-image the pump beam into the laser crystal. The pump spot radius, ω_p , was around 350 μm. The input mirror, M₁, was a 50 mm radius of-curvature concave mirror with antireflection coating at the diode wavelength on the entrance face ($R < 0.2\%$), high-reflection coating at lasing wavelength ($R > 99.8\%$) and high-transmission coating at the diode wavelength on the other surface ($T > 95\%$). Note that the laser crystal was placed very near the input mirror. The OPO cavity was formed by a coated KTP crystal and a coated Cr⁴⁺:YAG crystal. The 20-mm long KTP crystal was used in type II noncritical phase-matching configuration along the x-axis ($\theta = 90^\circ$ and $\phi = 0^\circ$) to have both a maximum effective nonlinear coefficient and no walk-off between the pump, signal, and idler beams. The KTP crystal was coated to have high reflectivity at the signal wavelength of 1573 nm ($R > 99.8\%$) and

high transmission at the pump wavelength of 1064 nm ($T > 95\%$). The other face of the KTP crystal was antireflection coated at 1573 and 1064 nm. The Cr^{4+} :YAG crystal has a thickness of 3 mm with 80% initial transmission at 1064 nm. One side of the Cr^{4+} :YAG crystal was coated so that it was nominally highly reflecting at 1064 nm ($R > 99.8\%$) and partially reflecting at 1573 nm ($R_s = 85\%$). The remaining side was antireflection coated at 1064 and 1573 nm. The overall Nd:YVO_4 laser cavity length was approximately 55 mm and the OPO cavity length was about 24 mm. As shown in the subsequent analysis, the present cavity length allows mode matching with the pump beam and provides the proper spot size in the saturable absorber.

6.3 Thermal Lens Effect Analysis of a Laser Crystal

The thermal lens of a laser crystal always affects the stability of a resonator, especially at a high pump power. An end-pump-induced thermal lens is not a perfect lens, but is rather an aberrated lens. It has been found that the thermally induced diffraction loss at a given pump power is a rapidly increasing function of mode-to-pump ratio. Practically, the optimum mode-to-pump ratio is in the range of about 0.6–1.0 when the incident pump power is greater than 5 W. For a fiber-coupled laser diode, the thermal lens can be given by [28]

$$\frac{1}{f_{th}} = \int_0^l \frac{\xi P_{in}}{2\pi K_c} \frac{\alpha e^{-\alpha z}}{1 - e^{-\alpha l}} \frac{[dn/dT + (n-1)\alpha_T]}{\omega_p^2 \{1 + [\lambda_p M_p^2 (z - z_0) / n\pi\omega_p^2]^2\}} dz \quad (6-1)$$

where ξ is the fractional thermal loading, K_c is the thermal conductivity, P_{in} is the incident pump power, n is the refractive indices along the c-axis of the Nd:YVO_4 crystal, dn/dT is the thermal-optic coefficients of n , α_T is the thermal expansion coefficient along the a-axis, l is the crystal length, ω_p is the radius at the waist, λ_p is the pump wavelength, M_p^2 is the pump beam quality factor, and z_0 is focal plane of the pump beam in the active medium. The first and second terms in the parenthesis of Eq.(6-1) arise from the thermal dispersion and the axial strain, respectively.

Considering the thermal lensing effect on the laser crystal, the mode beam radii ω_1 on the laser crystal and ω_2 on the saturable absorber can be given by [29]

$$\omega_i = \sqrt{\frac{\lambda L}{\pi}} \sqrt{\frac{g_j}{g_i(1-g_1g_2)}} \quad i, j = 1, 2; i \neq j \quad (6-2)$$

where $g_1 = 1 - (d_1 + d_2^*) / \rho_1 - d_2^* (1 - d_1 / \rho_1) / f_{th}$, $g_2 = 1 - d_1 / f_{th}$

$$L = d_1 + d_2^* - d_1 d_2^* / f_{th}, \quad d_2^* = d_2 + l_s (1/n_s - 1) + l_{KTP} (1/n_{KTP} - 1)$$

λ is the lasing wavelength, ρ_1 is the radius of curvature of the input mirror, d_1 and d_2 are the distances between the cavity mirrors and the principal planes of the laser crystal, n_s and n_{KTP} are, respectively, the refractive indices of the saturable absorber and the KTP crystal, and l_s and l_{KTP} are, respectively, the lengths of the saturable absorber and the KTP crystal. Note that the principal planes of the thermal lens can be approximated to be located inside the laser crystal at a distance $h = l/2n$ [29]. With Eqs. (6-1) and (6-2), the dependence of the mode size ratios ω_1/ω_p and ω_2/ω_1 on the pump power for the present cavity configuration was calculated and shown in Fig.6-2. The parameters used in the calculation are as follows: $\xi=0.24$,

$K_C=0.0523\text{W/K-cm}$, $\omega_p=0.35\text{mm}$, $M_p^2 \sim 310$, $d_1=2\text{mm}$, $d_2=48\text{mm}$, $\rho_1=50\text{mm}$, $n=2.165$, $n_s=1.82$, $n_{KTP}=1.745$, $l=7\text{mm}$, $l_{KTP}=20\text{mm}$, $l_s=3\text{mm}$, $dn_c/dT=3.0 \times 10^{-6}\text{K}^{-1}$, and $\alpha_T=4.43 \times 10^{-6}\text{K}^{-1}$. It is clear from Fig.5-2 that mode-to-pump size ratio ω_1/ω_p is around 0.6–1.0 for pump powers within 10–15 W, leading to optimal mode matching [26]. On the other hand, the ratio of the mode size in the saturable absorber and in the gain medium ω_2/ω_1 can be in the range of 0.1–0.3, satisfying the criterion for good passively Q-switching [30,31].

6.4 Criterion for Good Passively Q-Switching

The saturation of the pulse energy implies that the criterion for good passively Q-switching was entirely fulfilled. From the analysis of the coupled rate-equation, the criterion for good passively Q-switching is given by [32]

$$\frac{\ln\left(\frac{1}{T_0^2}\right)}{\ln\left(\frac{1}{T_0^2}\right) + \ln\left(\frac{1}{R}\right) + L} \frac{\sigma_{gs}}{\sigma} \frac{A}{A_s} \gg \frac{\gamma}{1-\beta} \quad (6-3)$$

where T_0 is the initial transmission of the saturable absorber, A/A_s is the ratio of the effective area in the gain medium and in the saturable absorber, R is the reflectivity of the output mirror, L is the non-saturable intracavity round-trip dissipative optical loss, σ_{gs} is the ground-state absorption cross-section of the saturable absorber, σ is the stimulated emission cross-section of the gain medium, γ is the inversion reduction factor with a value between 0 and 2 as discussed in [33], and β is the ratio of the excited-state absorption cross-section to that of the ground-state absorption in the saturable absorber. Since the σ value of the Nd:YVO₄ crystal ($25 \cdot 10^{-19} \text{cm}^2$) is comparable to the σ_{gs} value of the Cr⁴⁺:YAG crystal ($\sim(20 \pm 5) \cdot 10^{-19} \text{cm}^2$ [34]), the ratio $A/A_s = (\omega_1/\omega_2)^2$ generally needs to be greater than 10 for good passively Q-switching. As seen in Fig. 6-2, this criterion can be satisfied in the present cavity for pump power higher than 10 W. In other words, the experimental result consists very well with the theoretical analysis.

6.5 Experimental Results

Fig.6-3 shows the average output power at 1573 nm with respect to the incident pump power. For all pump powers the beam quality M^2 factor was found to be less than 1.3. The average output power reached 1.56 W at an incident pump power of 14.5 W. The conversion efficient from diode laser input power to OPO signal output power

was 10.8%. To the best of our knowledge, this is highest efficiency for average power conversion. The pulse temporal behavior at 1064 and 1573 nm was recorded by a LeCroy 9362 digital oscilloscope (500 MHz bandwidth) with a fast germanium photodiode. An oscilloscope trace of a train of the signal pulses is shown in the inset of Fig. 6-3. The pulse-to-pulse amplitude fluctuation was found to be within $\pm 10\%$

.Fig.6-4 depicts the pulse repetition rate and the pulse energy at 1573 nm versus the incident pump power. It is seen that the pulse repetition rate is proportional to the incident pump power and up to 58.5 kHz at an incident pump power of 14.5 W. On the other hand, the pulse energy initially increases with pump power, and is almost saturated beyond 10 W of the incident pump power.

A typical temporal shape for the laser and signal pulses is shown in the inset of Fig.6-4. It can be seen that the several satellite peaks accompany the main pulse whose pulse width is approximately 2.5 ns. Although the present output coupler reflectivity ($R_s = 85\%$) can lead to higher conversion efficiency, the stored energy is not fully extracted in a single output pulse. Since the remaining energy is sufficient to evolve the pump filed, the OPO threshold can be reached again and a second signal pulse is produced.

The energy in the satellites is about 30–40% of the total output energy. The output energy of the main pulse is estimated to be in the order of $15 \mu\text{J}$ at the pump power higher than 10 W. Therefore, the overall peak power can be higher than 5 kW. To produce a single pulse output, the OPO output reflectivity needs to be reduced to $<75\%$. As shown in Fig. 6-5, a single pulse can be generated with a signal reflectivity of 70% on the output coupler. Experimental results reveal that the maximum conversion efficiency can be obtained with an output coupler of 85–90% at the sacrifice of peak power. If the high peak power is desired, the output reflectivity needs to be around 60–70%.

6.6 Summary

In summary, a high-power efficient diode-pumped passively Q-switched Nd:YVO₄/KTP/ Cr⁴⁺:YAG eye-safe laser has been demonstrated by using a saturable

absorber Cr⁴⁺:YAG was coated as an output coupler of the OPO cavity to enhance the performance of passive Q-switching. Considering the thermal lensing effects, the cavity length was designed to allow mode matching with the pump beam and to provide the proper spot size in the saturable absorber. Consequently, the average output power at 1573 nm can amount to 1.56 W with a pulse repetition rate of 58.5 kHz and the peak power >5 kW at an incident pump power of 14.5 W.



References

- [1] R.C. Stoneman, L. Esterowitz, in: Proceedings of the Conference on Advanced Solid State Lasers, Optical Society of America, Washington, DC, 1990, p. 176, paper WC5-2.
- [2] P.F. Moulton, IEEE J. Quantum Electron. 21 (1985) 1582.
- [3] P.F. Moulton, A. Mooradian, Appl. Phys. Lett. 35 (1979)838.
- [4] S. Kück, K. Petermann, U. Pohlmann, G. Huber, Phys. Rev. B 51 (1995) 17323.
- [5] A. Sennaroglu, Prog. Quantum Electron. 26 (2002) 287.
- [6] B. Schmaul, G. Huber, R. Clausen, B. Chai, P. LikamWa, M. Bass, Appl. Phys. Lett. 62 (1993) 541.
- [7] M.V. Kuleshov, A.A. Lagatsky, A.V. Podlipensky, V.P. Mikhailov, A.A. Kornienko, E.B. Dunina, S. Hartung, G. Huber, J. Opt. Soc. Am. B 15 (1998) 1205.
- [8] I. Sokolska, E. Heumann, S. Kück, T. Lukasiewicz, Appl. Phys. B 71 (2000) 893.
- [9] A. Dening, P.E.-A. Möbert, G. Huber, J. Appl. Phys. 84(1998) 5900.
- [10] S. Taccheo, P. Laporta, S. Longhi, O. Svelto, C. Svelto, Appl. Phys. B 63 (1996) 425.
- [11] K.V. Yumashev, I.A. Denisov, N.N. Posnov, V.P. Mikhailov, R. Moncorge, D. Vivien, B. Ferrand, Y. Guyot, J. Opt. Soc. Am. B 16 (1999) 2189.
- [12] K. Spariosu, R.D. Stultz, M. Birnbaum, T.H. Allik, J.A. Hutchinson, Appl. Phys. Lett. 62 (1993) 2763.
- [13] R.D. Stultz, M.B. Camargo, M. Birnbaum, J. Appl. Phys. 78 (1995) 2959.
- [14] R.D. Stultz, M.B. Camargo, M. Lawler, D. Rockafellow, M. Birnbaum, in: W.R. Bosenberg, M.M. Fejer (Eds.), Advanced Solid State Lasers, OSA Trends in Optics and Photonics Series, vol. 19, Optical Society of America, Washington, DC, 1998, p. 155.

- [15] R.D. Stultz, M.B. Camargo, S.T. Montgomery, M. Birnbaum, K. Spariosu, *Appl. Phys. Lett.* 64 (1994) 948.
- [16] M. Birnbaum, M.B. Camargo, S. Lee, F. Unlu, R.D. Stultz, in: C.R. Pollock, W.R. Bosenberg (Eds.), *Advanced Solid State Lasers*, OSA Trends in Optics and Photonics Series, vol. 10, Optical Society of America, Washington, DC, 1997, p. 148.
- [17] R. Fluck, R. Häring, R. Paschotta, E. Gini, H. Melchior, U. Keller, *Appl. Phys. Lett.* 72 (1998) 3273.
- [18] J. Falk, J.M. Yarborough, E.O. Ammann, *IEEE J. Quantum Electron.* 7 (1971) 359.
- [19] R.S. Conroy, C.F. Rae, G.J. Friel, M.H. Dunn, B.D. Sinclair, J.M. Ley, *Opt. Lett.* 23 (1998) 1348.
- [20] A.R. Geiger, H. Hemmati, W.H. Farr, N.S. Prasad, *Opt. Lett.* 21 (1996) 201.
- [21] O.B. Jensen, T. Skettrup, O.B. Petersen, M.B. Larsen, *J. Opt. A: Pure Appl. Opt.* 4 (2002) 190.
- [22] J.J. Zayhowski, C. Dill III, *Opt. Lett.* 19 (1994) 1427.
- [23] Y.X. Bai, N. Wu, J. Zhang, J.Q. Li, S.Q. Li, J. Xu, P.Z. Deng, *Appl. Opt.* 36 (1997) 2468.
- [24] C. Li, J. Song, D. Shen, N.S. Kim, J. Lu, K. Ueda, *Appl. Phys. B* 70 (2000) 471.
- [25] Y.F. Chen, S.W. Chen, Y.C. Chen, Y.P. Lan, S.W. Tsai, *Appl. Phys. B* 77 (2003) 493.
- [26] Y.F. Chen, T.M. Huang, C.F. Kao, C.L. Wang, S.C. Wang, *IEEE J. Quantum Electron.* 33 (1997) 1424.
- [27] Y.F. Chen, *IEEE J. Quantum Electron.* 35 (1999) 234.
- [28] Y.F. Chen, T.M. Huang, C.C. Liao, Y.P. Lan, S.C. Wang, *IEEE Photon. Technol. Lett.* 11 (1997) 1241.
- [29] N. Hodgson, H. Weber, *Optical Resonators*, Springer-Verlag, Berlin, 1997.
- [30] A.E. Siegman, "Laser", University Science, Mill Valley, CA, 1986, pp. 1024 and

1012.

[31] Y.F. Chen, S.W. Tsai, IEEE J. Quantum Electron. 37(2001) 586.

[32] Y.F. Chen, Y.P. Lan, H.L. Chang, J. Quantum Electron.37 (2001) 462.

[33] J.J. Degnan, D.B. Coyle, R.B. Kay, IEEE J. Quantum Electron. 34 (1998) 887.

[34] G. Xiao, J.H. Lim, S. Ynag, E.V. Stryland, M. Bass, L.Weichman, IEEE J. Quantum Electron. 35 (1997)1086.



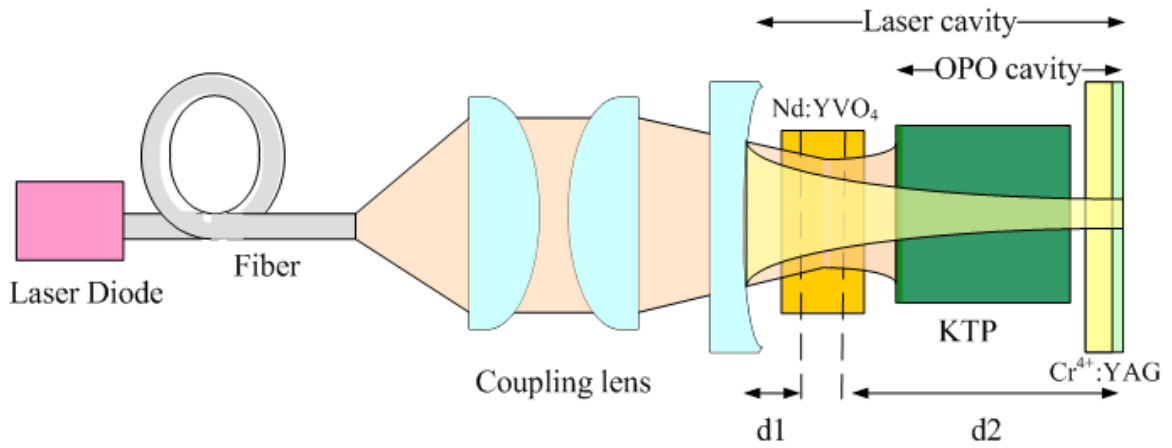


Fig.6-1 Schematic of the intracavity OPO pumped by a diodepumped passively Q-switched Nd:YVO₄/Cr⁴⁺:YAG laser.

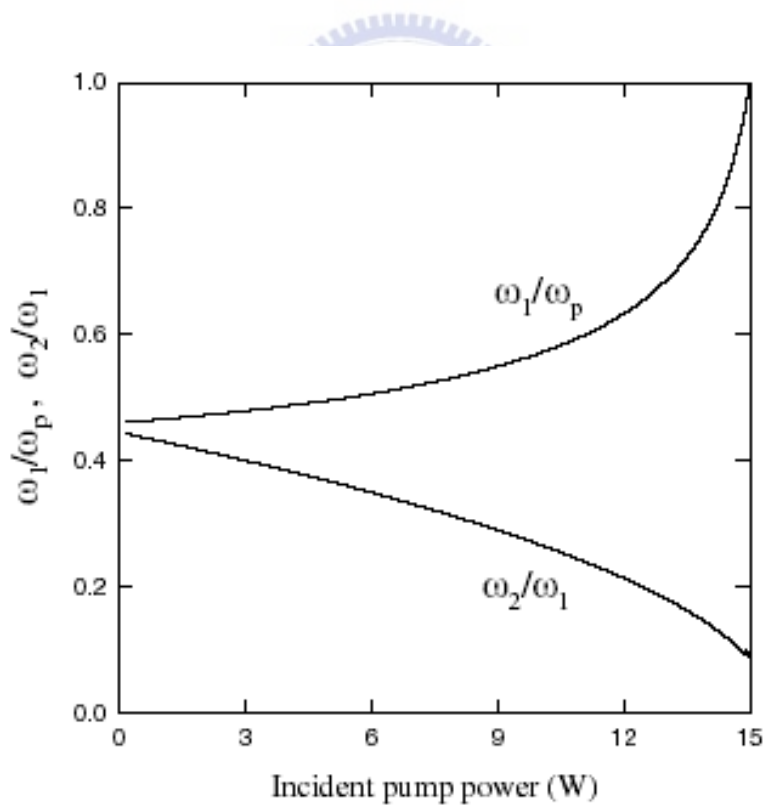


Fig.6-2 Calculation results for the dependence of the mode size ratios ω_1/ω_p and ω_2/ω_1 on the pump power for the present cavity configuration.

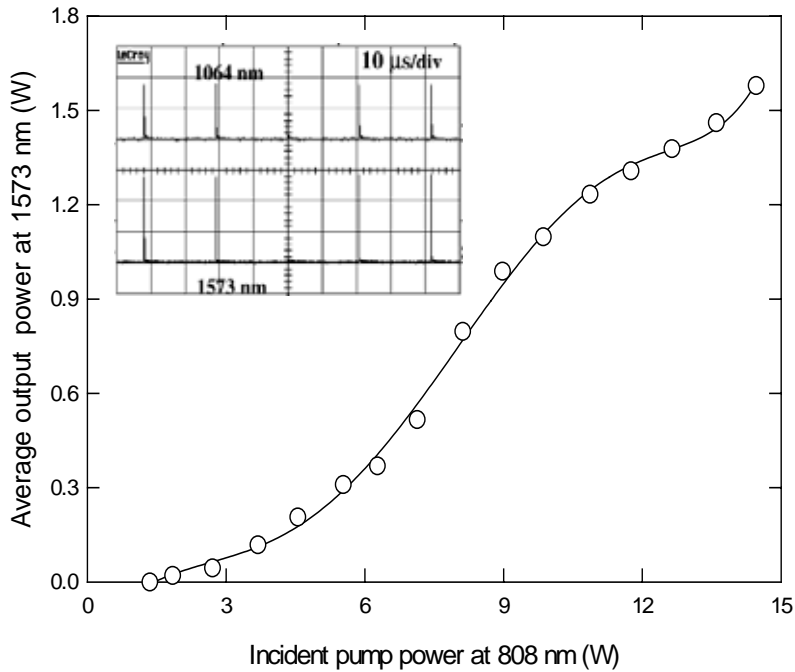


Fig.6-3 Dependence of the average output power at 1573 nm on the incident pump power. An oscilloscope trace of a train of the signal pulses is shown in the inset.

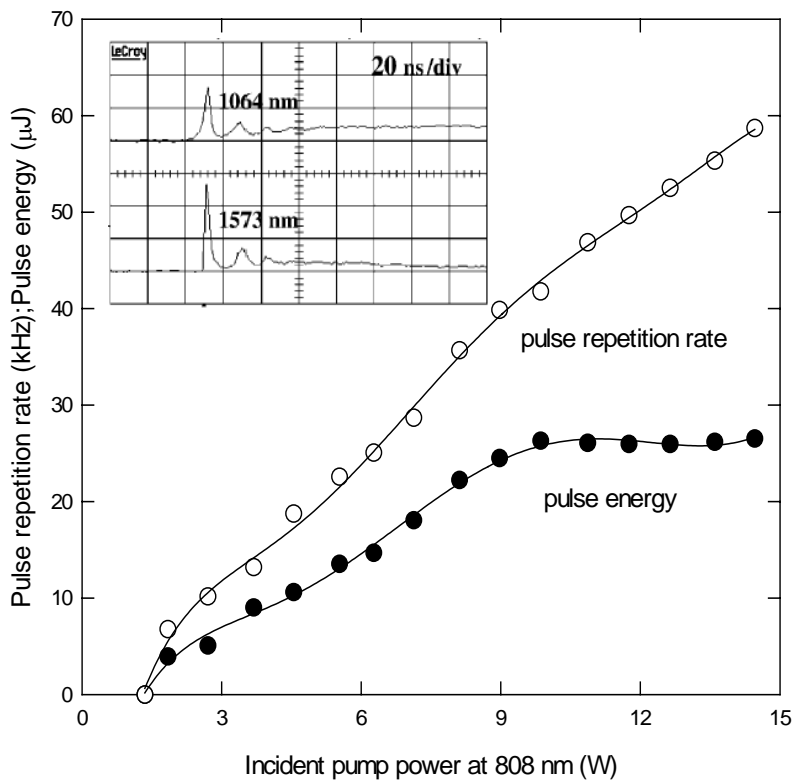


Fig.6-4 Dependence of the pulse repetition rate and the pulse energy at 1573 nm on the incident pump power. A typical temporal shape for the laser and signal pulses is shown in the inset.

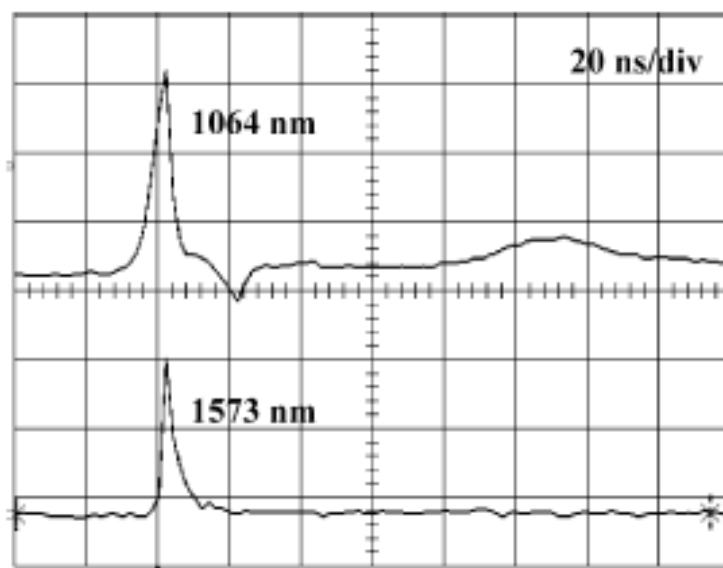
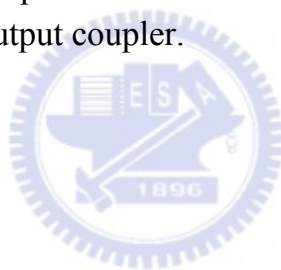


Fig. 6-5 Typical temporal shapes for the laser and signal pulses with a signal reflectivity of 70% on the output coupler.



Chapter 7 Conclusion and Future Work

This dissertation experimentally and analytically investigated the OPO design of several eye-safe solid-state lasers. In the active eye-safe lasers region, we experimentally accomplished an high-repetition-rate OPO by using a non-critically phase-matched KTP crystal intracavity pumped by an AO Q-switched Nd³⁺:YVO₄ laser. Operation of a singly resonant pulsed KTP intracavity OPO pumped by an AO Q-switched Nd:YVO₄ laser has been demonstrated. Using a type II non-critically phase-matched *x*-cut KTP crystal, eye-safe signal radiation at 1573 nm was generated in a plane-parallel to the intracavity OPO resonator. It was found that the maximum pulse energy may saturate beyond a given above-threshold intracavity OPO factor, but increasing the signal reflectivity of the output coupler can efficiently increases the average output power. The conversion efficiency for the average power is up to 10.6% from pump diode input to OPO signal output. The effective cavity dump of intracavity OPO leads to a relatively short signal pulse width for repetition rates from 10 to 80 kHz. As a consequence, the peak power for signal output can be up to several kilowatts for the entire frequency range. The compact size and high efficiency of the present laser make it an attractive source for practical applications.

The next topic was the study of the output optimization of a high-repetition-rate diode-pumped Q-switched intracavity optical parametric oscillator at 1573 nm with a type-II non-critically phase-matched *x*-cut KTP crystal. Numerical calculations have also been performed to confirm the experimental results. It was found that the maximum conversion efficiency can be obtained with an output coupler of 85%–90% at the cost of peak power. If high peak power is desired, the output reflectivity needs to be around 60%–70%.

In the passive eye-safe lasers region, the operation of a singly resonant pulsed KTP intracavity OPO pumped by a diode-pumped passively Q-switched Nd:YVO₄/Cr⁴⁺:YAG laser was demonstrated. A saturable absorber Cr⁴⁺:YAG was coated as an output coupler of the OPO cavity to constitute a realistic, inexpensive source of eye-safe nanosecond laser. The low threshold power permits the use of a relatively

low-power laser diode (2.5W). The conversion efficiency for the average power is up to 10.2% from pump diode input to OPO signal output. The effective cavity dump of intracavity OPO leads to the relatively short signal pulse width with high repetition rates. As a consequence, the signal peak power can exceed 1 kW with a pulse repetition rate of 62.5 kHz at an incident pump power of 2.5W

In the last, an efficient high-power diode-pumped passively Q-switched Nd:YVO₄/KTP/Cr⁴⁺:YAG eye-safe laser was accomplished by considering of the thermal lensing effects. The cavity length was designed to allow mode matching with the pump beam and provided the proper spot size in the saturable absorber. Consequently, the average output power at 1573 nm can amount to 1.56 W with a pulse repetition rate of 58.5 kHz and the peak power above 5 kW at an incident pump power of 14.5 W.

As the passively QS experimental results had revealed that shared cavity configuration has better stability performance, it will be worthwhile to apply the similar configuration to the actively Q-switched system and to use this configuration with PPLN to demonstrate the wavelength tunable IOPO configuration.

These compact and high-efficient eye-safe lasers introduce many potential applications studying in the future :

First, since they are more safe to human eyes, they can be developed to replace the traditional solid state lasers which have been used in commercial range finder and laser radar applications.

Second, after scaling up the output power, they can be used to remand the insufficiency of laser diode in the high-repetition-rate high-power application such as in laser indicator and active-imaging system.

Third, after militarizing these prototype system, they could be used for defense applications such as army tank or missile-borne or navy range finder, imaging system, etc.. Furthermore, the future study could improve the defense industry and promote the self-defense ability.